Dietrich, W. (1958). *Z. Physik* **152**, 306.
Dolby, R. M., and Swift, D.W. (1961) *Proc. European Regional Conf. Electron Microscopy, Delft*, 1960 Vol. 1, p. 114. Nederlandse Vereniging voor Electronenemicroscopie, Delft, Netherlands.
Duncumb, P., and Melford, D.A. (1960). "X-ray Microscopy and X-ray Microanalysis." Elsevier, Amsterdam.
Gleichauf, P. H. (1951). *J. Appl. Phys.* 22, 766.
Haine, M. E., and Cosslett, V. E. (1961) "The Electron Microscope." Spon, London.
Haine, M. E., and Einstein, P. A. (1952). *Brit. J. Appl. Phys.* **3**, 40.
Haine, M. E., Einstein, P. A., and Borchards, P. H. (1958). *Brit. J. Appl. Phys.* **9**, 482.
Hartwig, D., and Ulmer, K. (1963). *Z. Physik* **173**, 294.
Hibi, T. (1956a). *Proc. 3rd Intern. Conf. Electron Microscopy, London, 1954* p. 636 Roy. Microscop. Soc., London.
Hibi, T. (1956b). *J. Electronmicroscopy (Tokyo)* **4**, 10.
Hibi, T. (1962). *Proc. 5th Intern. Conf. Electron Microscopy, Philadelphia, 1962*, Vol. I, KK1. Academic Press, New York.
Hibi, T. (1964). *J. Electronmicroscopy (Tokyo)* **13**, 32.
Kofoid, M. J. (1960). *Trans. AIEE* **79**, Pt. III, 999.
Langmuir, D. B. (1937). *Proc. IRE* **25**, 977.
Niemeck, F. W., and Ruppin, D. (1954). *Z. angew. Phys.* **6**, 1.
Reimann, A.L. (1938). *Phil. Mag.* [7], **25**, 834.
Steigerwald, K. H. (1949). *Optik* **5**, 469.
Swift, D. W., and Nixon, W. C. (1962). *Brit. J. Appl. Phys.* **13**, 288.
Thon, F. (1963). *Zurich Cong.* p. 15. Abstract.

CHAPTER 2.2

ELECTROSTATIC LENSES

K.-J. Hanszen and R. Lauer
BRAUNSCHWEIG, GERMANY
PHYSIKALISCH-TECHNISCHE BUNDESANSTALT

2.2.1. General Properties of Image Formation

Any electrostatic field with rotational symmetry has imaging properties. Charged particles with equal energies, starting from points in the object plane, are focused into points in the (Gaussian) image plane if their paths are paraxial (that is, if they always run in a small distance from the axis and always have a small inclination to it). Rays such as this lead to a stigmatic (that is, a correct point-by-point) magnified or diminished image.

Magnification and position of the image depend on the energy of the particles: There is *energy dispersion*; the image formation is disturbed by *chromatic aberration*.

Off-axis rays are not focused into the same point as paraxial rays. The whole set of the intersection points of all adjacent rays starting from the same object point form a *caustic* shell: The image is affected by *geometrical aberrations.*

For *focusing* a beam with rotational symmetry, the area around the axis is utilized. With increasing demands on the imaging quality, the radius of the used lens area must be reduced. *Imaging with high resolution* (for example, in the electron microscope) requires an aperture, so small, that the diffraction at the edge of the diaphragm hole essentially influences the image quality. For *energy analyzing* (velocity spectrometry) one takes advantage of the strong chromatic aberration in the off-axis lens zones. Simultaneously, the particles with equal energy can be focused into a line focus on the caustic shell. Electrostatic lenses may also be used as *filter lenses*; with their aid it is possible to select the high energetical part of a beam.

A. Optical Lens Data

From the geometry of the lens electrodes, in principle it is possible (a) to determine the potential- and field-distribution in the lens and (b) from these, to determine all possible electron paths. In many cases, however, for the description of the paraxial lens data, it is sufficient to know only the paths of two paraxial rays entering the lens in parallel to the axis from the right hand side and the left hand side, respectively. Then the so-called "cardinal points"—which can be determined mostly by direct experiments —totally describe the image formation. Therefore, we shall concern ourselves foremost with these cardinal points. Without restriction we admit that the particles have different energies in front of and behind the lens. Consequently all equations are valid for immersion lenses too (see Section 2.2.2,B).

1. *Cardinal Points*

Particularly important for the description of the imaging conditions in the case of field-free object and image spaces are the axis coordinates of the following points:[1]

(a) The z coordinates z_{H*} and $z_{H'*}$ of the intersection points of the entrance and exit asymptotes of rays entering the lens parallel to the axis from the right- and left-hand side, respectively;

[1] In order to give f and f' the same sign, the values for the axis coordinates on the object and image side increase in the opposite direction (see Figs.). Always, when H, F, and f cannot be *strictly* regarded as cardinal elements, they will be marked by asterisks.

(b) The intersection points z_{F*} and $z_{F'*}$ of the exit asymptotes of the same rays mentioned in (a) with the axis of the lens;

(c) The coordinate differences $z_{F*} - z_{H*} =_{df} f^*$ and $z_{F'*} - z_{H'*} =_{df} f'^*$.

Applying these expressions to paraxial rays according to Fig. 1, we will omit the asterisks and notate the coordinates of the *principal planes* as z_H and $z_{H'}$; the coordinates of the *focal planes* as z_F and $z_{F'}$; and the corresponding focal lengths of the object and image side as f and f', respectively. We call the whole of these data as (*virtual*) *cardinal points* (Glaser, 1952, 1956).

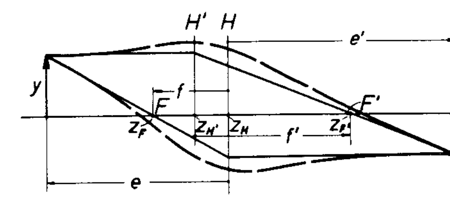

FIG. 1. Construction of the virtual cardinal points by the aid of the entrance and exit asymptotes. z_F and $z_{F'}$ are the axis coordinates of the virtual focal points F and F' on the object and image side, z_H and $z_{H'}$ the axis coordinates of the corresponding principal planes.

With the aid of these cardinal points, it is possible to determine *in field-free object and image spaces* the corresponding image distance e' and the lateral magnification M' (negative sign for inverted imaging!)

$$M' =_{df} \frac{y'}{y} \quad (y = \text{object size}; \quad y' = \text{image size}) \tag{1}$$

of the Gaussian image from the equation

$$\frac{f}{e-f} = \frac{e'-f'}{f'} = -\frac{y'}{y} \quad \text{for any object distance } e. \tag{2}$$

The *power* K of a lens is defined by

$$K =_{df} \pm 1/(ff')^{1/2} \text{ (positive sign for } f, f' > 0\text{; negative sign for } f, f' < 0). \tag{3}$$

Between the focal lengths f; f' and the kinetic energies W; W' of the particles in front of and behind the lens, the fundamental equation (Glaser, 1952, see p. 150)

$$\frac{f'}{f} = \left(\frac{W'(1 + W'/2\,W_0)}{W\,(1 + W\,/2\,W_0)}\right)^{1/2} =_{df} \left(\frac{W_r'}{W_r}\right)^{1/2} \tag{4}$$

with W; W' = kinetic energies, see (44); and

$$W_0 = \text{rest energy } m_0 c_0^2$$

is valid. From this, we obtain for the nonrelativistic case (W; $W' \ll W_0$):

$$\frac{f'}{f} = \left(\frac{W'}{W}\right)^{1/2} \tag{4a}$$

Hence the focal lengths f, f' differ only for immersion lenses; they are equal for single lenses. For these the following relation holds:

$$K = 1/f = 1/f' \tag{5}$$

Usually the object and the image screen are located outside the field, because, otherwise, they would raise field deformations. Under these circumstances, (2) is always applicable. For image formation by means of several stages, however, the intermediate images may be located in the field of a subsequent lens.

In such cases, we can apply other cardinal points: the so-called *osculatory cardinal points* (Glaser, 1952, 1956); the scope of these points is limited however to a small interval of object displacements. Numerical information about the osculatory cardinal points of electrostatic lenses are not published.

2. *Operating Ranges of a Lens*

Except gauze lenses (Sections 2.2.2,A,3; 2.2.2,B,1), which raise particular problems, weak lenses always have the properties of converging lenses, but never those of diverging lenses. The principal planes coincide ("thin lenses"). With increasing excitation the principal planes withdraw from each other ("thick lenses"). Their position is always inverted, see Fig. 1. In strong lenses the point of intersection of parallel incident rays can move into the lens field, so as to produce a second or even a third crossover by subsequent focusing (see Fig. 2). According to the number of existing crossovers the operating ranges will be of first, second, or third order, respectively. Negative focal lengths occur in the operating range of second-order.

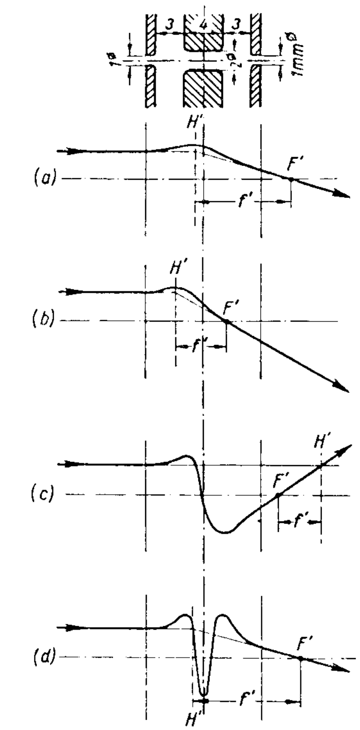

FIG. 2. Particle trajectory and positions of the image side focal and principal points of an electrostatic single lens according to Heise and Rang (1949). The electrical excitation increases from Fig. 2a to Fig. 2d (a, b first operating range, c second range, d third range). The whole focal and principal point characteristic of this lens is given in Fig. 9, the power characteristic in Fig. 20.

3. *Paraxial Chromatic Aberration*

Because of the chromatic lens aberration (see the beginning of this chapter), an image aberration disk of radius δ_{ch} is formed in the Gaussian image plane. Introducing the relative energy width $\Delta W/W$ of the particles and the angle of incidence α, we can establish the following relation:

$$\delta_{ch} = \alpha\, c_{ch} \frac{\Delta W}{W} \tag{6}$$

c_{ch} is called the *chromatic aberration constant related to the image.* The radius of the image aberration disk corresponds to the interval ε_{ch} in the object plane

$$\varepsilon_{ch} = \frac{\delta_{ch}}{M'} = \alpha \frac{c_{ch}}{M'} \frac{\Delta W}{W} = \alpha C_{ch} \frac{\Delta W}{W} \tag{7}$$

where M' is the lateral magnification and

$$C_{ch} =_{df} c_{ch}/M' \tag{8}$$

C_{ch} is called the *chromatic aberration constant related to the object.* Both constants depend on the object position (and thus on the magnification too). Particles with high energy always intersect the axis at larger distances behind the lens (see Fig. 3b) than those with low energy.

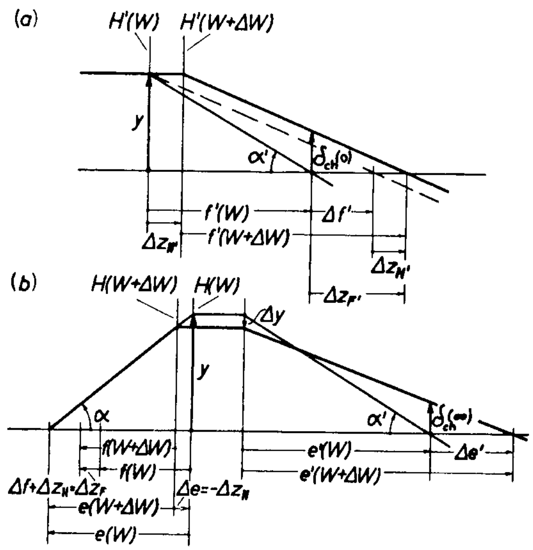

FIG. 3. Chromatic aberration disk δ_{ch} and chromatic focal point displacements Δz_F, $\Delta z_{F'}$ (a) for very strong diminution; and (b) for very strong magnification.

The chromatic aberration in the paraxial area may also be described by the energy dependence of the coordinates of the focal and principal points. With very strong diminution ($M' \to 0$) and with very strong magnification ($M' \to \infty$), very simple mathematical conditions emerge.

(a) $M' \to 0$ The incident beam can be regarded as a beam of parallel rays. As shown in Fig. 3a, δ_{ch} is only given by the displacement of the cardinal elements $\Delta z_{H'}$ and $\Delta f'$ of the image space. We find

$$\delta_{ch}(0) = \frac{y}{f'(W + \Delta W)} \cdot \Delta z_{F'} = \frac{y}{f'(W + \Delta W)} (\Delta f' + \Delta z_{H'}) \tag{9}$$

with $f'(W + \Delta W) = f'(W) + \Delta f'$.

For $\Delta f' \ll f'$ and for small angles of emersion α', Eq. (9) becomes

$$\delta_{ch}(0) = \frac{y}{f'(W)} \cdot \Delta z_{F'} = \alpha' \, \Delta z_{F'}; \qquad \varepsilon_{ch}(0) = \frac{\alpha'}{M'} \Delta z_{F'} \tag{10}$$

Considering the Helmholtz-Lagrange formula

$$M' = -\frac{\alpha}{\alpha'} \left(\frac{W_r}{W_r'} \right)^{1/2} \tag{11}$$

and comparing (10) with (7), we shall get the required relation between the chromatic aberration constant $C_{ch}^{(0)}$ and the chromatic aberration $\Delta z_{F'}$ the rear focal point

$$C_{ch}(0) = -\frac{\Delta z_{F'}(W_r/W_r')^{1/2}}{M'^2 \, \Delta W/W} \tag{12}$$

(b) $M' \to \infty$ Since the object distance e does not differ from f practically, the emerging beam may be interpreted as a beam of parallel rays. Now the image distance e' is so large that we can equate $e' - f' \approx e'$ and the displacement of the coordinates of the principal and focal points on the image side will be of no importance. As shown in Fig. 3b, for the radius of the chromatic-aberration disk, we may write

$$\delta_{ch}(\infty) = \frac{y + \Delta y}{e' + \Delta e'} \Delta e' \approx \frac{y}{e'} \Delta e' = \alpha' \, \Delta e' \tag{13}$$

if $\Delta y \ll y$, $\Delta e' \ll e'$. e' is regarded here as a function of e, f, and f'.
In this manner we obtain with (1) and (2) the total differential of e':

$$\begin{aligned}\Delta e' &= M'\left[\frac{f'}{e-f}(\Delta e - \Delta f) - \Delta f'\right] = -M'\left[\frac{f'}{e-f}\Delta z_F + \Delta f'\right] \\ &\approx -M'\Delta z_F \, \alpha/\alpha' = -M'\Delta z_F \, e'/f\end{aligned} \tag{14}$$

considering (1) - (4); (11) and

$$\Delta e = -\Delta z_H; \; \Delta f - \Delta e = \Delta z_F; \; \Delta f' = \Delta f (W_r'/W_r)^{1/2} \tag{15}$$

Substituting (14) into (13) and converting it to $\varepsilon_{ch}(\infty)$, we get

$$\delta_{ch}(\infty) = -(y/f)M' \, \Delta z_F = -\alpha M' \, \Delta z_F; \qquad \varepsilon_{ch}(\infty) = -\alpha \, \Delta z_F \tag{16}$$

Comparing this result with (7), we find the required relation between the chromatic-aberration constant $C_{ch}(\infty)$ and the chromatic aberration Δz_F of the focal point on the object side:

$$C_{ch}(\infty) = -\frac{\Delta z_F}{\Delta W/W} \tag{17}$$

c. *Inversed Ray Tracing.* In opposition to our former procedure the rays now shall enter from the right-hand side. In this case we must convert all the symbols with primes into the symbols without primes. The symbols of the corresponding chromatic-aberration disks will be indicated by the letter u. With

$$M \underset{df}{=} \frac{1}{M'} = -\frac{\alpha'}{\alpha}\left(\frac{W_r'}{W_r}\right)^{1/2} \tag{18}$$

we obtain

$$\delta^u_{ch}(0) = \alpha\,\Delta z_F \quad ; \quad \varepsilon^u_{ch}(0) = \frac{\alpha}{M}\,\Delta z_F \tag{19}$$

$$\delta^u_{ch}(\infty) = -\alpha' M\,\Delta z_{F'} \quad ; \quad \varepsilon^u_{ch}(\infty) = -\alpha'\,\Delta z_{F'} \tag{20}$$

Especially the combination of (19), (16), (17) leads to the result

$$\varepsilon_{ch}(\infty) = -\delta^u_{ch}(0) = C_{ch}(\infty)\,\alpha \cdot \Delta W/W \tag{21}$$

Hence, the chromatic aberration constant for *strong magnification* can be determined by using the inversed ray tracing with strong diminution. This method is analogous to the method for determining the spherical aberration (see Section 2.2.1,A,5c).

4. *General Information about Off-Axis Data*

In discussing the data about the off-axis lens zones, again we confine ourselves to field-free object and image spaces. It is sufficient to know the entrance asymptotes and the corresponding exit asymptotes of each ray. The entrance asymptote is characterized (see Fig. 4a) by its *intersection point p with the axis* and by its *slope* $\tan \alpha = y/(p-q)$; the exit asymptote (see Fig. 4a) is characterized by its *intersection point* p' *with the axis* and its *slope* $\tan \alpha' = y'/(p'-q')$. The asymptotes of rays incident parallel to the axis are characterized by their *heights of incidence* y instead of by their slopes $\tan \alpha$ (Hanszen, 1958b).

Only in the paraxial area, the data of all rays in a beam emitted by a point source in any finite distance from the lens can be evaluated by the data of an incident and an emerging ray both parallel to the axis (see Fig. 1). As to the off-axis lens zones this is not possible. In order to know the lens properties completely, it is indispensable to measure or calculate the entrance and exit asymptotes for all possible rays. Moreover, on account of the chromatic errors, these measurements or calculations have to be done for particles of different energies. Mostly, however, it is sufficient to determine only the data of a beam that emerges from a *fixed* point source (necessarily not located on the axis) and to evaluate from these the interesting *geometrical aberrations*. The data derived in this manner are not confined to an approximate theory of aberrations.

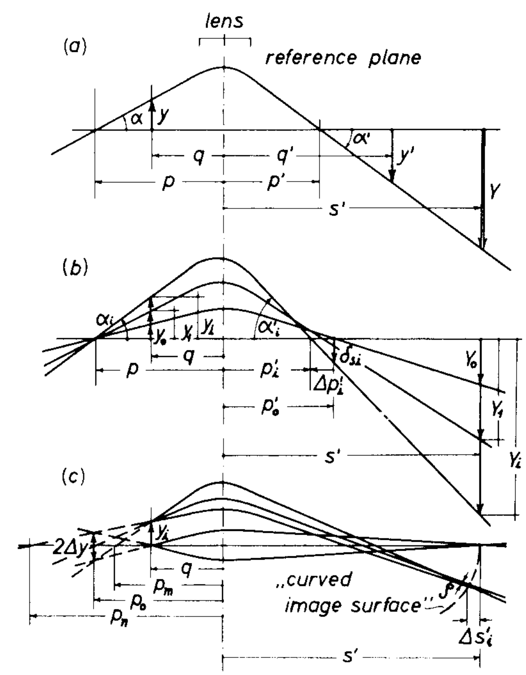

Fig. 4. Ray tracing in the off-axis lens zones.

a. *Spherical Aberration.* The intersection point with the axis p_i' on the image side and the angle of emersion α_i', belonging to the rays originating from an axis point with the fixed coordinate p, depend only on the specific angle of incidence α_i (and for parallel rays on the heights of incidence y_i), see Fig. 4b. If we take the axis point p to be an object point, then p_i' is the corresponding image point, and, especially, for $a \to 0$, $p_i' \to p_0'$ it is the corresponding (paraxial) Gaussian image point. Then

$$\Delta p_i' =_{df} p_i' - p_0' \tag{22}$$

is the *spherical longitudinal aberration* (see Fig. 25) and

$$\delta_{s_i} =_{df} \Delta p_i' \tan \alpha_i' \tag{23}$$

is the *radius of the spherical-aberration disk*. Both are defining quantities for the spherical aberration. As we will learn from the next section, the spherical aberration is closely connected with the distortion.

b. *Distortion.* We consider the points $(q, 0)$; (q, y_0); . . . ; (q, y_i) to be point sources of very narrow beams, the chief rays of which are drawn in Fig. 4b; two beams are exactly drawn up in Fig. 4c. Beams such as this originate from each object point, if an object at a distance q is illuminated by a source of finite diameter $2\,\Delta y$ located at a distance p.

The Gaussian image of $(q, 0)$ will be located at $(s', 0)$. Then, the image of the plane $(z = q, y)$ lying in the plane $(z = s', Y)$ is distorted. The same error, which is outstanding for the spherical aberration if an object point at the distance p—acting as a pupil—is imaged in the Gaussian image plane at the distance p', produces a distortion in another plane at the distance s', if the object is located at another distance q and if the entrance pupil is located at the distance p.

c. *Field Curvature, Coma, Off-Axis Astigmatism.* Figure 4c shows how to derive the field curvature (curvature of the "image surface," marked by $\Delta s_i'$) and the *coma* (marked by ϱ) from the hitherto drawn rays.

Rays originating from the same object point, which do not proceed in the drawing plane, are not imaged in the same surface. The deviation of this surface from the one drawn describes the *off-axis astigmatism.*

d. *Summary.* Except for the off-axis astigmatism, which is not only determined by the rays proceeding in the plane of incidence, we can characterize all geometrical aberrations according to Fig. 4a by the intersection points and the slopes of the entrance and exit asymptotes of all rays in the system. Hence it is, for example, sufficient to know the cardinal points and the spherical aberrations in the form of $\Delta p'(\alpha)$ and $\delta_s(\alpha)$ for the rays with all possible axis intersections p_m, p_n, p_0, . . . in order to determine distortion, field curvature, and coma.

5. *Third-Order Aberrations*

In the lens zones immediately annexed to the paraxial area (in the so-called Seidel area), we are allowed to make further statements about the geometrical aberrations, if we expand the deviation of the off-axis image points from the paraxial image points into a series and consider only the first term. In this article we will do this only for the spherical aberration and the distortion. But first, we will point out the relation between spherical aberration and distortion that holds in this area.

a. *Relations between the Spherical-Aberration Disk for Very High Diminution and the Distortion of a Shadow Image at a Large Distance.* According to Fig. 4b, we project the shadow image of an object located at the distance q, by a point source at the distance $p \to \infty$. The image screen will arbitrarily be placed at a large distance s'. According to the particulars of Fig. 5, the exit

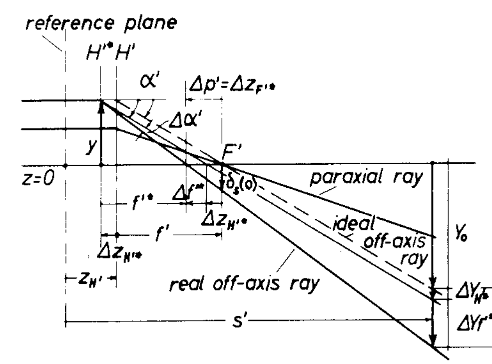

FIG. 5. Spherical aberration disk $\delta_s(0)$ for strong diminution and the distortion $\Delta Y/Y_0$.

asymptote of a ray, entering parallely with a great height y of incidence into an aberration-free lens, intersects the axis at the focal point F' of the image side with the slope $\tan \alpha' = y/f'$. The ray emerging from an imperfect lens[2] differs from this ray by a longitudinal displacement $\Delta z_{H'*}$ and by a variation $\Delta\alpha'$ of the angle of emersion α'. This variation leads to a displacement $\Delta f'^*$ of the intersection point with the axis. Thus the total displacement of this point, that is, the longitudinal spherical aberration, amounts to

$$\Delta p' = \Delta z_{H'*} + \Delta f'^* = \Delta z_{F'*} . \tag{24}$$

[2] As to the following notations, see Section 2.2.1,A,1. The asterisked quantities are derived in the same manner as the cardinal points from the entrance and exit asymptotes of an parallel incident beam, but they do not establish an imaging in the sense of Eq. (2).

The radius of the spherical aberration disk has the value

$$\delta_s(0) = \Delta z_{H'*} \tan \alpha' + \Delta f'^* \tan(\alpha' + \Delta\alpha') \approx$$
$$(\Delta z_{H'*} + \Delta f'^*) \tan \alpha' = \Delta z_{F'*} \cdot \tan \alpha'. \qquad (25)$$

The second line of equation (25) holds as long as $\Delta\alpha' \ll \alpha'$. Similarly, we can write for the distortion with reference to Fig. 5

$$\frac{\Delta Y}{Y_0} = \frac{\Delta Y_{H'*}}{Y_0} + \frac{\Delta Y_{f'*}}{Y_0} \approx \frac{\Delta z_{H'*} + (s' - z_{H'})\,\Delta f'^*/f'}{Y_0} \cdot \tan \alpha', \qquad (26)$$

whereas $Y_0 = -(s' - z_{H'} - f')\tan\alpha'$. If $(s' - z_{H'}) \gg f'$, the first term of the numerator of Eq. (26) can be neglected with respect to the second one. Then, we obtain for the distortion

$$\Delta Y / Y_0 \approx -\Delta f'^*/f'. \qquad (27)$$

The image-aberration disk is characterized by the *total* longitudinal aberration $\Delta z_{F'*}$ according to (25), whereas, the distortion is marked mainly by a part of the longitudinal aberration, namely, by $\Delta f'^* = \Delta z_{F'*} - \Delta z_{H'*}$. This is to say, the size of the spherical-aberration disk is essentially given by the displacement of the axis intersection $\Delta z_{F'*}$, whereas the distortion is chiefly expressed by the variation $\Delta\alpha'$ of the ray's slope and therefore by $\Delta f'^*$. From this we recognize the great difficulty in the *exact* determination of the spherical aberration from the distortion. Moreover, it is difficult to fix $z_{F'*}$ accurately. The published values, however, are mostly due to such measurements.

b. *The Spherical-Aberration Disk for Very Strong Magnification.* For $M' \to \infty$ the intersection of an incident paraxial ray with the axis (signed by terms with the subscript 0) coincides with the first focal point. The corresponding ray of emersion is nearly parallel to the axis. With the analogous approximations in reference to the image side, as made in 2.2.1,A,3b, we can write for the radius of the image-aberration disk (see Fig. 6)

$$\frac{\delta_s(\infty)}{\Delta e'} = \frac{y_1}{e'(\alpha_0) + \Delta e'} \approx \frac{y_1}{e'(\alpha_0)} \qquad (28)$$

A ray emerging from a large distance y_1 parallel to the axis (represented in Fig. 6 with sufficient approximation by the line —·—) may intersect the axis on the object side in F^*. We assume its distance from the focal point to be Δz_{F*}. In spite of the impossibility in describing the imaging properties

of the off-axial lens zones by the aid of the virtual cardinal points, we assume that between the rays $\overparen{FH^*ED_1}$ and $\overparen{F^*H^*ED_0}$ there is an, at least, osculatory dependence in accordance with the lens equation. Then, in the

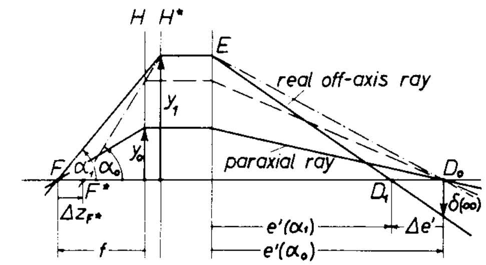

FIG. 6. Spherical aberration disk $\delta_s(\infty)$ for strong magnification. (In order to get a clear drawing the object distance e is equated with the focal length f.)

same procedure and with the same restrictions as in 2.2.1,A,3b, we can write analogously to (14)

$$\Delta e' = -M' \Delta z_{F*} e'/f: \qquad (29)$$

Applying (28), we obtain in this manner for the radius of the aberration disk

$$\delta_s(\infty) = -y_1 M' \Delta z_{F*}/f = -\alpha M' \Delta z_{F*} \qquad (30)$$

c. *The Constants of Spherical Aberration.* For the radius of the spherical-aberration disk, the following expansion is valid:

$$\delta_s = c_s \alpha^3 + \cdots \qquad (31)$$

where c_s is the *spherical aberration constant related to the image*. The radius of the image-aberration disk corresponds to the interval on the object side:

$$\varepsilon_s = \frac{\delta_s}{M'} = \frac{c_s \alpha^3}{M'} + \cdots \quad =_{df} C_s \alpha^3 + \cdots \qquad (32)$$

Here

$$C_s = c_s / M' \qquad (33)$$

is the *spherical-aberration constant, related to the object*.

The values of these two aberration constants depend on the object position and thus on the magnification. For *strong diminution* we obtain with (11), (25), (31), and for very small α, the following connection between the aberration constant related to the object $C_s(0)$ and the longitudinal aberration $\Delta z_{F'*}$ the following relation:

$$C_s(0) = -\frac{\Delta z_{F'*}}{M'^2\alpha^2}\cdot\left(\frac{W_r}{W_r'}\right)^{1/2} \tag{34}$$

Similarly, we obtain with (30) for strong magnification:

$$C_s(\infty) = -\,\Delta z_{F*}/\alpha^2 \tag{35}$$

As in Section 2.2.1,A,3c we can relate our considerations to the inversed ray tracing again. Instead of (25) and (30) with (32), and (18), for very small α, the following equations result:

$$\delta_s^u(0) = \alpha\,\Delta z_{F*} \quad ; \quad \varepsilon_s^u(0) = \frac{\alpha}{M}\,\Delta z_{F*} \tag{36}$$

$$\delta_s^u(\infty) = -\,\alpha' M\,\Delta z_{F'*} \quad ; \quad \varepsilon_s^u(\infty) = -\,\alpha'\,\Delta z_{F'*} \tag{37}$$

$$C_s^u(\infty) = -\,\Delta z_{F'*}/\alpha'^2 \tag{38}$$

Of special interest is the comparison between (30) and (36). Considering (32), we have for very small α

$$\varepsilon_s(\infty) = -\,\delta_s^u(0) = -\,\alpha\,\Delta z_{F*} = C_s(\infty)\alpha^3 \tag{39}$$

Hence it is possible to determine the "spherical-aberration constant related to the object $C_s(\infty)$ for infinite magnification and object position on the unprimed lens side" from the displacement of the axis intersection Δz_{F*} belonging to this side. There are two different ways to determine Δz_{F*}: *either* from $\delta_s(\infty) = \varepsilon_s(\infty)M'$ in the direct ray tracing with very strong magnification, *or* from $\delta_s^u(0)$ in the inversed ray tracing (that is, incidence on the primed side) with very strong diminution.

On the same way we can derive from (25) and (37) two methods for the determination of the spherical-aberration constant $C_s^u(\infty)$ belonging to the other lens side. For these we obtain

$$\varepsilon_s^u(\infty) = -\,\delta_s(0) = -\,\alpha'\Delta z_{F'*} = C_s^u(\infty)\alpha'^3 \tag{40}$$

The given relations that do not depend on alterations of the particles' energies, are *valid for immersion lenses* too.

Trajectories with greater angle of incidence intersect the axis always in shorter distances behind the lens than trajectories with smaller angle of incidence (Exception: gauze lenses, see 2.2.2,A,3).

d. *The Constant for Distortion.* For the distortion we can give the following expansion:

$$\frac{\Delta Y}{Y_0} = c_d\,\alpha'^2 + \cdots \tag{41}$$

From this, in the special case of (27) we have for the distortion constant c_d

$$c_d = -\frac{\Delta f'^*}{f'\,\alpha'^2}. \tag{42}$$

Measured values for this constant, will be given in 2.2.2,A,2d.

6. *Experimental Methods*

Fortunately, we are able to rely on extensive direct experimental material for the data of electrostatic lenses. We will consult these measurements as much as possible and comment on the performed comparison between theory and experiment in suitable passages herein. Next, we will give a short outline of the experimental measuring methods in use. More details about measuring arrangements may be drawn from the original literature.

a. *General Methods.* As mentioned in 2.2.1,A,4, the most general method of measuring the lens data is based on determining all correlated couples of entrance and exit asymptotes in a beam. In the further description we use the notations of Fig. 4a,b. The source of the beam is placed at the distance p in front of the lens. (We are mostly interested in $p \to \infty$; see 2.2.1,A,5a,c). The most exact method in determining the functions $\tan\alpha'$ $(\tan\alpha)$ and $p'(\tan\alpha)$, which fix the required asymptotes, is demonstrated in Fig. 7. In the planes with the axis coordinates q and q' we successively displace a diaphragm with a fine hole along the coordinates y and y', respectively, and register each shadow image of the hole on a photographic plate, the translation of which in x direction is coupled linearly with the diaphragm movement (see Hanszen, 1964a;c). The curves, plotted in this way, give information about $Y(y)$ and $Y(y')$, their mutual correlation gives the wanted connections directly (see Figs. 23–26). Measurements such as these enable us to evaluate, particularly, the paraxial and the Seidel data.

b. *Determination of the Cardinal Points.* The former method is also suitable for determining the positions of the principal and focal points, because the coordinate $z_{F'}$ of the focus on the image side can be found from an incident parallel beam ($p \to \infty$) by $z_{F'} = p'(y \to 0)$, and similarly the corresponding focal length f', by

$$f' = \lim_{y \to 0} \frac{y}{\tan \alpha'} \quad ; \quad \text{with} \quad \alpha' = \alpha'(y) \tag{43}$$

In order to determine the positions of the principal and focal points on the object side, we have to use the inversed ray tracing (in the case of symmetrical single lenses, we need of course with $f = f'$ and $z_H = z_{H'}$ only one measuring procedure).

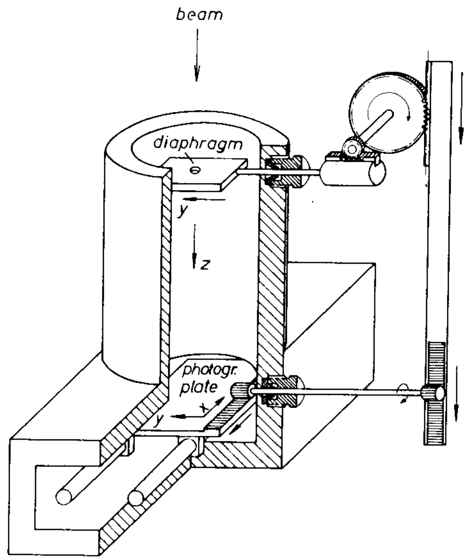

FIG. 7. Measurement of the rays' exit asymptotes by coupling the movement of a fine hole along the y coordinate with the translation in x direction of a photographic plate, which registrates the shadow image of the hole (Hanszen, 1964a).

If our intention is to determine only the paraxial lens data, it is sufficient for us to use a more simple arrangement in which the shadow magnifications of two small objects (such as thin wires) are measured; the first of them is placed before the lens and the second behind it in the distances q and q', respectively (Klemperer and Wright, 1939; Spangenberg and Field, 1942; Heise and Rang, 1949; Liebmann, 1949; Everitt and Hanszen, 1956; Septier, 1960; Fink and Kessler, 1963; Hamisch and Oldenburg, 1964).

For asymmetrical lenses, *two measuring procedures* are required again. In this case there is no need to place the source at a *large* distance from the lens. As shown by Everitt and Hanszen (1956), simply, the lens must be turned around the intersection point of the reference plane and the optical axis between the two measurements. In doing this, the electrodes of immersion lenses must keep their original potentials. Very simple equations result if $q = q'$ and $p = s'$ are chosen.

c. *Determination of Distortion and Spherical Aberration.* In order to determine the distortion by the above shadow method, we have to introduce extended objects into a practically parallel incident beam in front of the lens [with advantages: nets (Heise, 1949; Jacob and Schah, 1953); rows of teeth (Hanszen, 1958b); rows of holes, movable edge (Liebmann, 1949)]. The shadow image of these objects at very large distances s' behind the lens delivers the information (41) about *the distortion.* With the general method 2.2.1,A,6a, the relative distortion for large s' can be read off immediately from the deviation of the registrated curves from a straight line.

By employing the exact formula (24) to (26), (39), (40), the data for the *spherical-aberration disk* (and thus for the longitudinal spherical aberration) can be determined in the same way from the distortion (considerations concerning the exactness of this method are pointed out in Section 2.2.1,A,5a). Particularly, the spherical aberration constant for strong magnification $C_s(\infty)$ can be determined by the inversed ray tracing. But the accuracy of these measured values is not high at all. It must be emphasized that this method allows us to measure $C_s(\infty)$ for a (virtual) object position in the lens field too. But this case is hardly of any practical advantage since for objects in the lens field the osculatory cardinal elements are decisive instead of the virtual ones.

In the *direct methods* of determining the spherical-aberration constant for strong magnification, the exit asymptote is measured in direct dependence on the angle of incidence using the normal ray tracing. According to Seeliger (1948), Shipley (1952), and Septier (1960), a fine hole, placed at the intersection point of the axis with the first focal plane, is irradiated under various inclinations α. Thus, the spherical aberration constant $C_s(\infty)$ can be calculated from the positions of the corresponding exit asymptotes. This method is only valid if the focal points are located out of the lens field.

Mahl and Recknagel (1944) employed as "electron pencils" the diffraction intensities emitted into discrete glancing angles by a microcrystalline object, positioned on the axis. With this method, the spherical aberration can be determined from the distortion of the Debye-Scherrer-diagram in the focal plane of the image side.

B. Similarity Laws

For nonrelativistic velocities of the particles, the properties of an electrostatic lens are only determined by the mutual *ratio* R of the electrode-potentials referred to the particles' rest potential U_0, but not by the absolute values of the electrode potentials. Under these circumstances, particularly the particles' trajectories are independent of the ratio: particle charge to particle mass. Hence, we shall introduce in the following passages a suitable *voltage ratio* R as an electric parameter. We shall call the dependences of the optical quantities on R, the "*characteristics*"; for example, $K(R) = 1/[ff'(R)]^{1/2}$ will be called the lens power characteristic, and so on. For relativistic velocities, however, the trajectories of the particles depend on the ratio of kinetic energy to rest energy. Then, the trajectories are not only functions of the voltage ratio, but also of the absolute values of the individual voltages. Data for a special lens are given in 2.2.2,A,2b.

In lenses with *similar geometry*, operating at the same ratio R, all particles describe similar paths. In this case, we are able to give the geometrical lens data, in a reduced scale; that is, the required data will be divided by a significant length (for example, electrode distance, bore diameter or focal-length). Since in the relativistic range, only particles with the same ratio of kinetic energy to rest energy describe similar paths, the reduced geometrical lens data are functions of this ratio.

C. Confrontation of Electrostatic and Magnetic Lenses

1. *Consequences Taken from the Ray Equations*

In electrostatic lenses the trajectories of particles with nonrelativistic velocities and with the same ratio of kinetic energy to electric charge, that is, particles which have passed the same accelerating voltage, are independent of the particles' mass. In magnetic fields, however, under the same conditions the particle trajectories depend on the particles' mass: Heavy particles in particular are less focused than light ones. On that account, electrostatic lenses are favored to focus *heavy particles* (*ions*).

2. *Consequences Taken from the Equation of Motion*

Whereas the kinetic energy

$$W = e(U_0 - U) \tag{44}$$

(where e is the charge of the particles, U_0 the equilibrium rest potential of the particles, and U the electrostatic potential at the considered point) of a particle does not alter along the whole path in the field of a magnetic lens, in the electrostatic lens field considerable energy alterations are possible. By an opposing field of sufficient strength the particles may even be reflected instead of being transmitted. In a beam with particles of equal energy this is done in the off-axis lens zones by a lower opposing electrode potential than in the paraxial zone. This effect is relevant for the action of the grid in electron guns as "iris diaphragm." In beams with particles of different energies, the particles with the lower energy likewise are reflected by a lower opposing potential. In this case, the lens has filtering properties (see Section 2.2.2,A,5d).

If the particles endure energy alterations only in the lens field (then their energy is the same on both lens sides, and object and image space have the same electrostatic potential), we call these lenses "*single-lenses*." For these we must substitute $W = W'$ in all equations. Especially the two focal lengths f and f' are equal, see Eq. (4). If the electrostatic potentials in the object and image space are different, we have *accelerating* or *decelerating lenses*. For both, we use the notion "*immersion lenses*." In the following section the data of single and immersion lenses are referred to separately.

3. *Consequences of the Object Position*

In order to avoid deformations of the imaging field, the objects are not allowed, particularly for strong magnifications, to immerse into the imaging field of electrostatic lenses. With the exception of ferromagnetic materials, however, the objects are generally allowed to immerse into the imaging field of magnetic lenses. This leads to the following consequences:

a. *Applicability of the Virtual Cardinal Points to Electrostatic and Magnetic Lenses*. The virtual cardinal points, the applicability of which is confined to field-free object and image spaces, are of main importance for electrostatic lenses, but of secondary importance for magnetic lenses. Since the virtual cardinal points can be easily derived from the course of the asymptotes by experiments, the experimental methods for determining the lens data—in opposition to the analytical methods—are more relevant for electrostatic than for magnetic lenses.

b. *Applicability of Electrostatic and Magnetic Lenses as Microscope Objectives*. As pointed out in 2.2.2,A,5a, on account of the demand for field-free object position and the requirement of high-voltage technology (2.2.3,A,B), only a minimum focal length about 6 mm of electrostatic objective lenses can be reached, whereas magnetic lenses with focal lengths 2 mm or less are commonly in use. Moreover, it is not possible to reduce the spherical aberration of the objective, which is decisive for the resolving power of transmission microscopes, to its minimum value in electrostatic objectives. Therefore these lenses are not adequate for high-resolution microscopes (particulars are reported in 2.2.2,A,2c and 2.2.2,A,5a).

4. *Consequences Taken from Designing*

From the examples of Section 2.2.3,C, it follows, that electrostatic lenses mostly can be more simply manufactured than magnetic lenses. On that account, for more simple experiments in laboratories the electrostatic lenses are often favored above magnetic lenses. But their limited high-tension rigidity is a great disadvantage. It is unpromising to operate high-voltage lenses with short focal lengths by much more than 60 kV.

2.2.2. Data of Particular Lenses

In most cases electrostatic lenses are realized by a sequence of coaxially arranged tubes or diaphragms on different electrostatic potentials. Complicated geometries only exceptionally occur. If one or several lens electrodes are equipped with gauzes, which must be crossed by the beam, we call these lenses *gauze-lenses*. We shall deal with them in connection with the belonging diaphragm and tube lenses.

A. Single Lenses

Single lenses may be realized by three-diaphragm or three-tube systems, whose external electrodes have the same potential U_a as the field-free external spaces. We call the potential of the intermediate electrode U_i.

According to the performance of Section 2.2.1,B, the electrical excitation will be designated by the characteristic voltage ratio

$$R_{sl} = \frac{U_i - U_0}{U_a - U_0} \tag{45}$$

Mostly, the potential of the intermediate electrode has such a sign that the particles are decelerated in the field between entrance and intermediate electrode. Then the operating voltage ratio is $R_{sl} < 1$. In this case, the potential of the intermediate electrode can be drawn from the high-tension generator, which supplies the accelerating voltage. Owing to the low energy of the particles near the intermediate electrode, lenses operating at a voltage ratio smaller than 1 by the amount x have considerably stronger power than lenses operating at a voltage ratio greater than 1 by the amount x.

Moreover, for the realization of voltage ratios $R_{sl} > 1$, an additional high-voltage supply is needed.

1. *An Illustrative Model of the Single Lens*

With voltage-ratios $R_{sl} < 1$, the potential distribution around the intermediate electrode of an electrostatic single lens acts as converging lens; the potential distributions around the external electrodes act as diverging lenses. With $R_{sl} > 1$, the conditions are just opposite. For details see 2.2.2,B,2. But always the converging parts of the potential field are predominant; thus the whole lens always acts as a converging lens. For qualitative considerations the diverging part can be thoroughly neglected.

Real diverging lenses can be realized only by suppressing the converging part of the potential distribution. This can be done for $R_{sl} < 1$ by replacing the intermediate aperture electrode by a conducting, but transparent foil (for practical purposes represented by fine gauzes). Since all parts of the potential distribution for $R_{sl} > 1$ act inversed, the lens with the above gauze electrode operates at this voltage ratio as a converging lens. All other lenses in the first operating range are always converging lenses (see Section 2.2.1, A,2), irrespective of $R_{sl} \lessgtr 1$ (that is, $U_i \lessgtr U_a$). Both focal lengths of these lenses are equal. In the operating ranges of higher order the lens power may

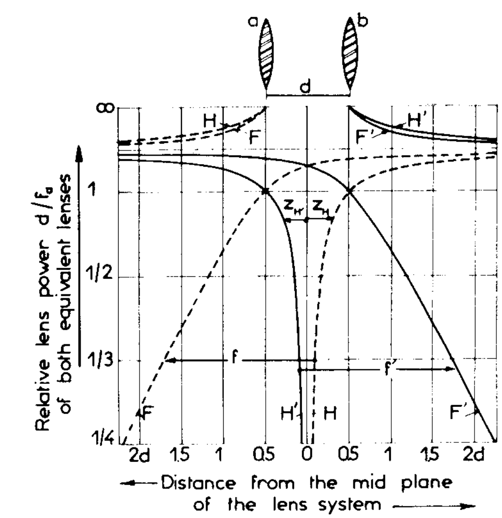

Fig. 8. Entire course of the focal and principal-point coordinates of a lens system consisting of two equal weak converging lenses a and b with the fixed mutual distance d in dependence of the lens power $1/f_a = 1/f_b$ belonging to each lens (Hanszen, 1958a).

increase in such a degree that several successive focusings occur (see Fig. 2). An illustrative model for the influence of the increasing electrical excitation on the cardinal points in the first and second operating range represents a system of two thin "equivalent lenses" a and b, placed at the fixed mutual distance d, whose lens powers $1/f_a$ and $1/f_b$ increase in a constant ratio (Hanszen, 1958a; Felici, 1959; there are given further mathematical evaluations). Symmetrical single lenses, that is, lenses whose intermediate electrode lies in a symmetry plane, may be represented by two "equivalent lenses" with equal lens powers $1/f_a = 1/f_b$ thusly (see Fig. 8; compare a real characteristic of cardinal points, for example, Fig. 9).

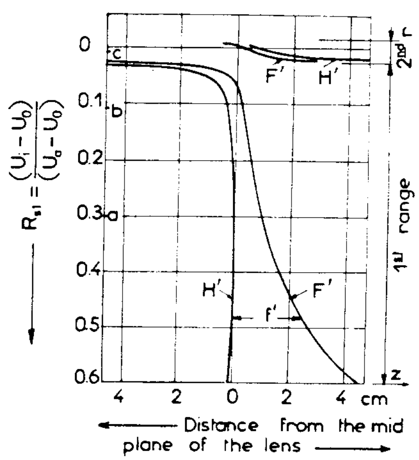

FIG. 9. Entire course of the focal and principal point coordinates (focal and principal point characteristics) of the lens shown in Fig. 2 in dependence of the voltage ratio R_{sl} for the first and second operating range, according to Heise and Rang (1949) (U_i = potential of the intermediate electrode, U_a = potential of the outer electrodes, U_0 = rest potential of the particles, z = axis coordinate). The voltage ratios which refer to the trajectories a and b of Fig. 2 are marked on the ordinate scale. The cardinal points on the object side and the cardinal point on the image side lie symmetrically to the midplane of the lens. The power characteristic of this lens is represented in Fig. 20.

2. *Three-Diaphragm Single Lenses*

As to three-diaphragm single lenses, extensive theoretical calculations have been done (Regenstreif, 1951; Glaser and Schiske, 1954, 1955; Kanaya *et al.*, 1966). The ray tracing in these lenses also has been investigated with the aid of analogical systems (electrolytic trough, resistor network, and so on). But there exist such a lot of direct measurements that we exclusively can relate on these in the following sections. Comparison with the other

methods may be drawn from Lippert and Pohlit (1954), Archard (1956), and Vine (1960).

a. *Characteristics of Lens Power. Focal Points and Principal Points.* The following geometrical parameters influence the cardinal points decisively:

(a) The distances a and a' between the intermediate and the external electrodes;

(b) The thickness d of the intermediate electrode;

(c) The diameter b (and possibly the geometrical shape) of the aperture in the intermediate electrode.

The dependence of the cardinal points on the voltage $R_{sl} < 1$ is demonstrated for various lenses in Figs. 9–16. Special interest requires the general

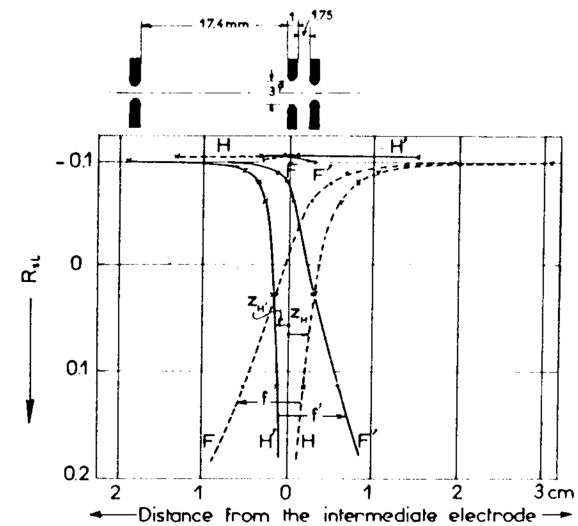

FIG. 10. Focal and principal point characteristics of the drawn asymmetrical lens (Everitt and Hanszen, 1956).

behavior of the lens power characteristics $1/f(R_{sl})$. With increasing electric excitation, that is, with decreasing voltage ratio downward from $R_{sl} = 1$, we find in the Figs. 11 to 16 the first operating range with $1/f > 0$, which is followed by the second operating range with $1/f < 0$. For some lenses even operating ranges of higher order with alternating sign of the lens power have been observed. Between each two consecutive operating ranges there is a *telescopic operating point* with $1/f = 0$. Figures 11–13 (similar as Fig. 9) refer on *symmetrical single lenses*. They show the influence of several geometrical shape parameters. The lenses with the first maximum of the lens power at $R_{sl} = 0$ are particularly interesting. The geometrical data of these lenses may be taken from Fig. 14.

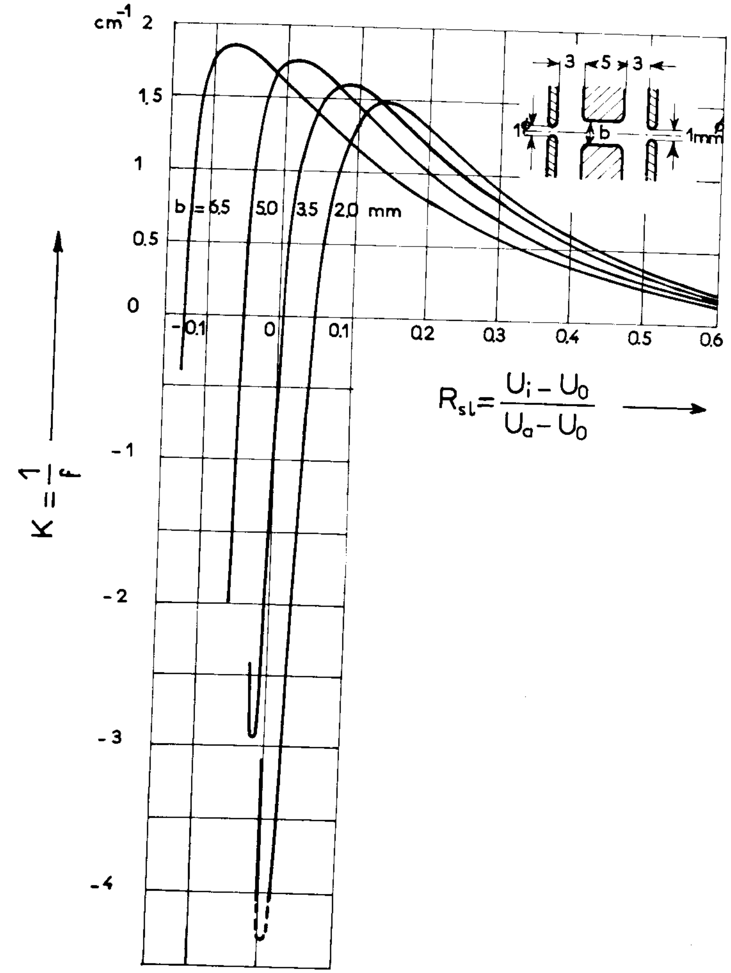

FIG. 11. Power characteristics of symmetrical single lenses. Parameter is the bore diameter b of the intermediate electrode (Heise and Rang, 1949).

Asymmetrical single lenses are expediently discussed in connection with symmetrical single lenses; their properties can be derived from the properties of the latter by varying a single parameter (for example, the ratio of the electrode distances a'/a) *under maintenance of the first telescopic operating*

point (Everitt and Hanszen, 1956). Both focal lengths of asymmetrical single lenses are equal too. Figures 15 and 16 show some lens power characteristics. The power maximum of the asymmetrical lens is reached almost at the same voltage ratio as the maximum of the corresponding symmetrical lens and is somewhat higher than the latter. The position of the principal planes of these lenses is no longer symmetrical with respect to the intermediate electrode (see Fig. 10). The "midplane of the lens" appears displaced towards the side with the higher potential gradient.

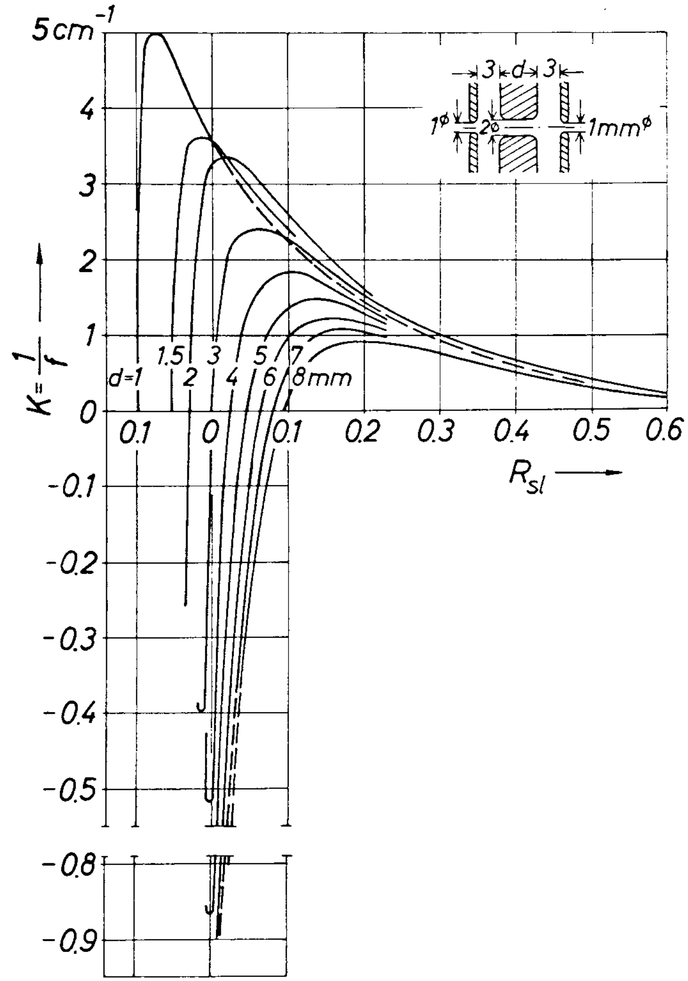

FIG. 12. Power characteristics of symmetrical single lenses. Parameter is the thickness d of the intermediate electrode (Heise and Rang, 1949).

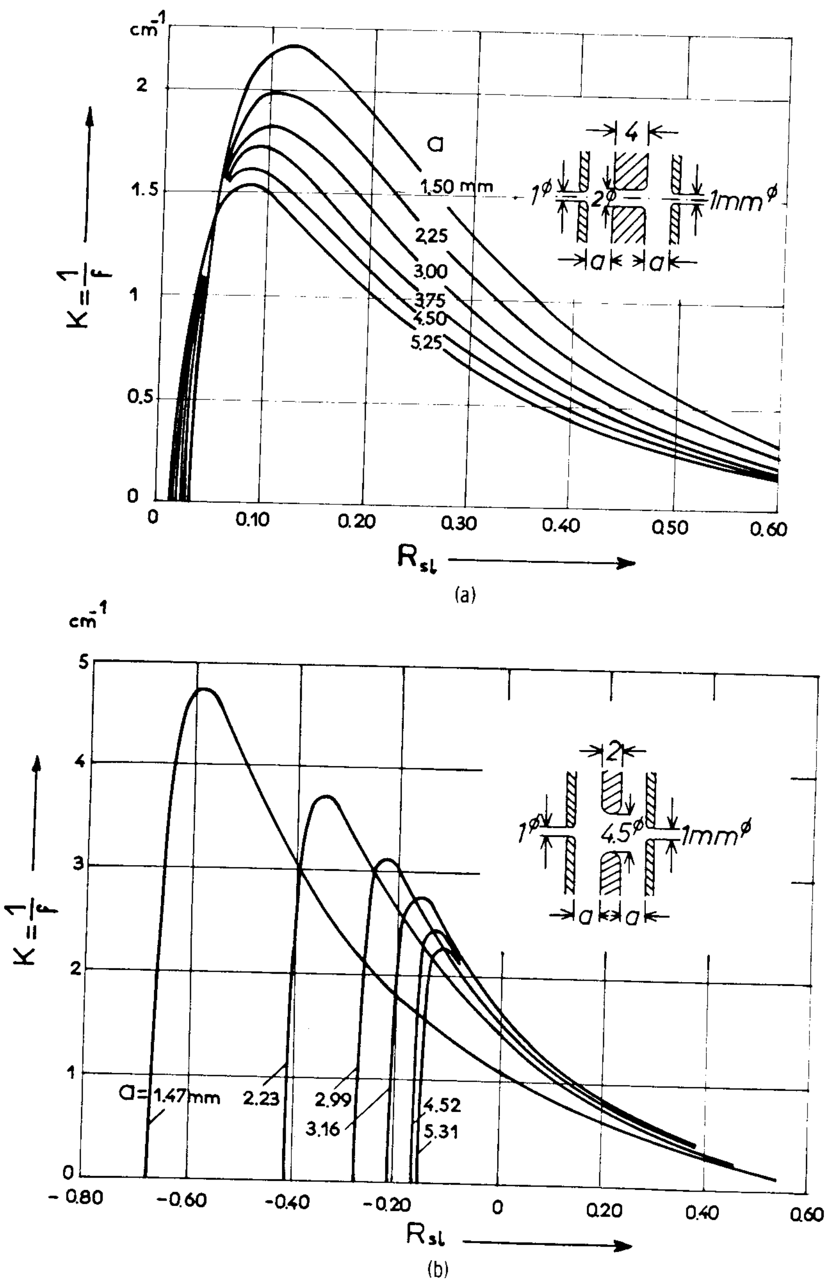

FIG. 13. Power characteristics of symmetrical single lenses (a) with a narrow bore in a thick intermediate electrode and (b) with a wide bore in a thin intermediate electrode. Parameter is the electrode distance a (Heise and Rang, 1949).

b. *Cardinal Points of Unipotential Lenses.* Very simple relations result, if the potential of intermediate electrode is equal to the rest potential of the particles, for in this case R_{sl} has the constant value 0 for all accelerating voltages $U_a - U_0$. Therefore, the cardinal points of these lenses, for particles with nonrelativistic velocities, do not depend on the amount of the accelerating voltage. We call these lenses *unipotential lenses.*

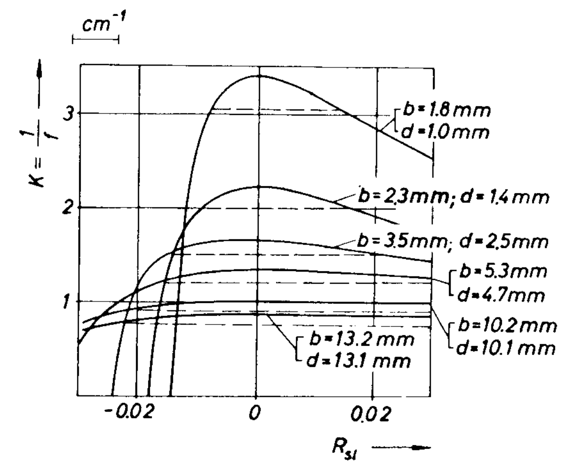

FIG. 14. Lens power of symmetrical single lenses with the first power maximum at $R_{sl} = 0$ (that is, operating as unipotential lens). The R_{sl} interval in which the power decreases by 10% is plotted with dotted lines (Lippert and Pohlit, 1952); b is the bore diameter; d the thickness of the intermediate electrode; and a the distance of the electrodes. The lens length $l = 2a + d$ of all treated lenses amounts to 20 mm.

The manner in which the lens power $K = 1/f$ of symmetrical unipotential lenses depends on the geometrical data is shown in Fig. 17; the manner in which the focal point coordinates z_F depend on the same data is given in Fig. 18. The solid curves refer to the first, the dotted curves to the second operating range. The comparison of both figures leads to the following statement: For distances $> 0.5l$ between the focal points and the midplane of the lens (that is, focal points beyond the lens field) and for a fixed position of the focal points, the focal length—and the positions of the principal planes too—are nearly independent of the geometrical data b/l and d/l of the intermediate electrode. It is easy to understand that this behavior occurs in the first operating range in as much as the principal planes are located close to the midplane and the conditions of weak lenses exist. As calculated by Laplume (1947), in the relativistic range the focal length of unipotential lenses first increases approximately 8% with increasing beam

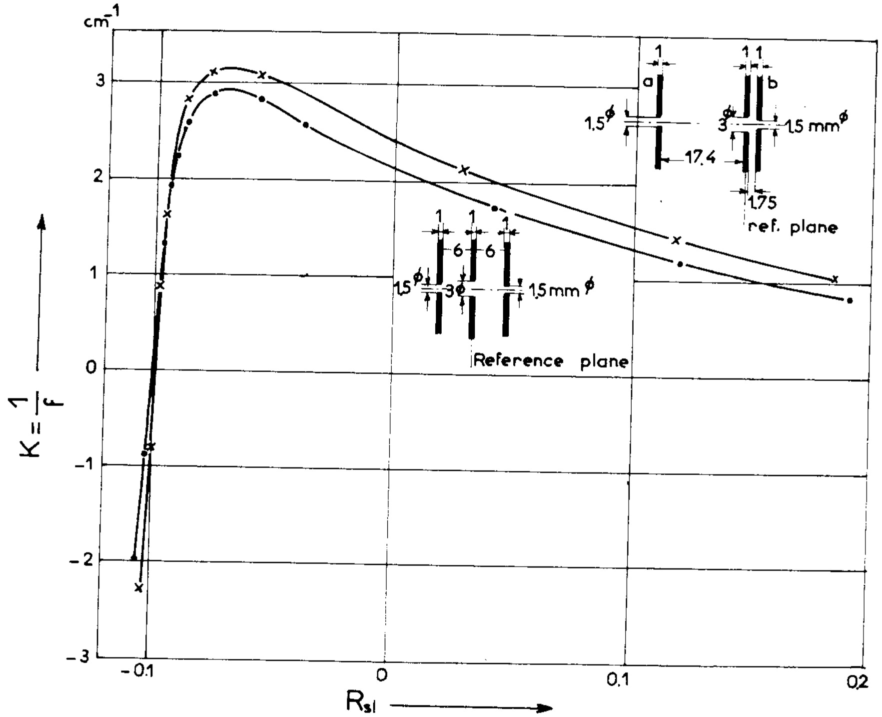

FIG. 15. Lens power characteristics of an asymmetrical single lens and of a symmetrical single lens with the same telescopic operating point (Everitt and Hanszen, 1956).

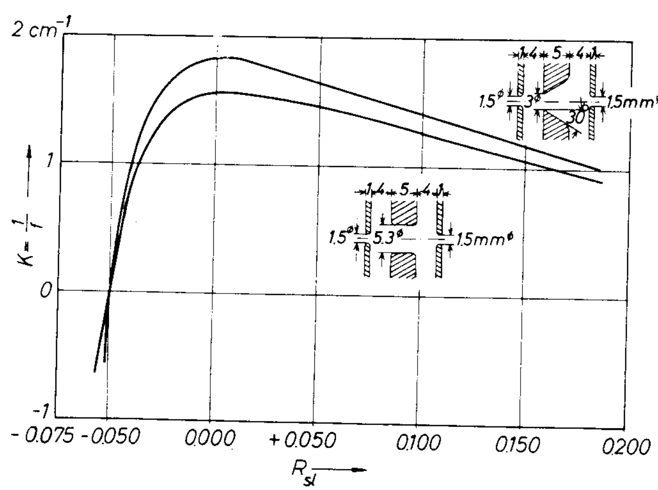

FIG. 16. Lens power characteristics of an asymmetrical and a symmetrical single lens with equal telescopic operating points (Hanszen, 1958a).

energy until a maximum is reached for electrons with the kinetic energy of 1 MeV. With still higher energies, the focal length decreases again and with energies of 5 MeV it falls even below the nonrelativistic value of the focal length; for still higher energies a finite boundary value is reached. The distance of the principal planes from the midplane changes in the opposite sense as the focal length. Their displacements however are, by far, smaller.

c. *Chromatic Aberration of Single Lenses.* The particles within a beam have a finite energy width $\Delta W = e\,\Delta U_0$ because of their different rest energies. Since U_0 is connected with R_{sl} according to (45), the cardinal points for particles with different energies of incidence can be determined from the given information about the lens characteristics, respecting the validity of

$$\Delta R_{sl} = \Delta W/W\,(1 - R_{sl}) \tag{46}$$

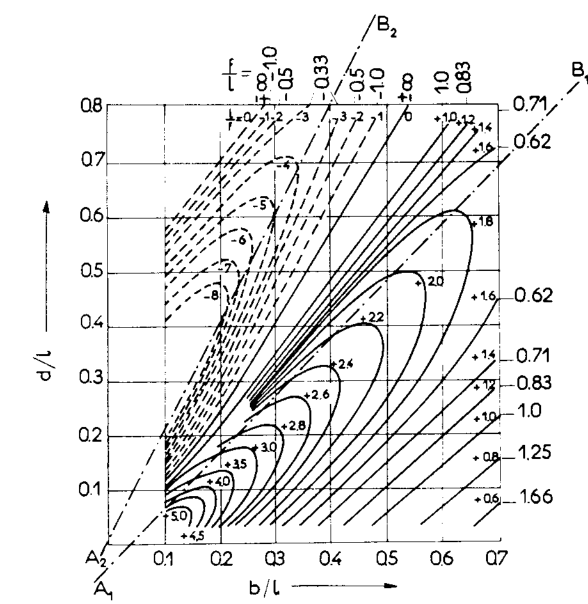

FIG. 17. Dependence of the relative lens power l/f and of the relative focal length f/l of symmetrical unipotential lenses ($l = 2a + d$ = lens length) on the relative geometrical lens data (see Figs. 12 to 14) according to Lippert and Pohlit (1952) (b is the bore diameter of the intermediate electrode; d the thickness of the intermediate electrode; and a the distance of the electrodes). Solid curves = 1st operating range; dotted curves = 2nd operating range. The straight line A_1B_1 marks the first lens power maximum; the line A_2B_2 marks the second power maximum. Both maxima are characterized by focal length achromatism. Curves with the parameter value $l/f = 0$ (that is $f/l = \pm\infty$) mark the telescopic operating points.

and particularly for unipotential lenses with $R_{sl} = 0$ of

$$\Delta R_{sl} = \Delta W/W \tag{47}$$

Since the chromatic-aberration constants are determined by the chromatic displacements Δz_F and $\Delta z_{F'}$ of the focal points [compare, (12), (17)], the constants of chromatic aberration can be evaluated directly from the focal point characteristics (for example, Figs. 9 and 10). In this manner, the "chromatic-aberration constant related to the object for strong magnification" $C_{ch}(\infty)$ for single lenses (that is, for $W = W'$) can be expressed by the equation

$$C_{ch}(\infty) = \frac{\Delta z_F}{\Delta W/W} = \frac{\Delta z_F}{\Delta R_{sl}}(1 - R_{sl}) \tag{48}$$

and particularly for unipotential lenses by

$$C_{ch}(\infty) = \frac{\Delta z_F}{\Delta R_{sl}} \tag{49}$$

With this we directly learn from Fig. 10, that the chromatic aberration of asymmetrical single lenses is unequal on both lens sides.

Because $\Delta z_F/\Delta R_{sl}$ does not vanish anywhere, the chromatic aberration does not vanish at any operating point too. According to Fig. 3, we can

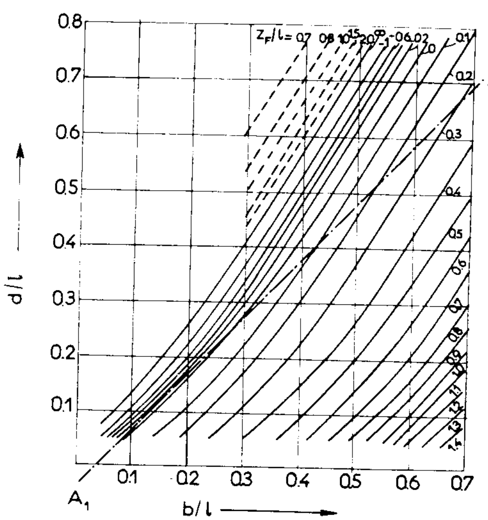

FIG. 18. Dependence of the relative focal point coordinates z_F/l on the geometrical lens data (Lippert and Pohlit, 1952). Notations as in Fig. 17; the origin of the coordinate system is located in the lens center.

see that the displacements Δz_F and $\Delta z_{F'}$ of the focal points are the sum of the displacement of the principal points Δz_H and $\Delta z_{H'}$ and the alter ation of the focal lengths Δf and $\Delta f'$, respectively. The latter vanish a the maximum of the lens power (at this points we have *focal-length* achro matism). For this reason, the chromatic error reaches its minimum val ue near this point—or, strictly speaking, at an operating point just below the power maximum. The flatter the maximum, the wider the range around the maximum with low chromatic aberration (see Fig. 14). Another chro matic error is the *chromatic error of magnification*. It depends essentiall on the position of the exit pupil (Wendt, 1940; Hanszen and Lauer, 1965) If the pupil is located at the second focal plane, for strong magnifications this error is given by $\Delta f/f$, that is, by the lens power characteristic. Th chromatic error of magnification vanishes for an appropriate position of th pupil. For initially decelerating lenses, the ratio $C_{ch}(\infty)/f$ decreases if th electrical excitation decreases and runs to 2 for $R_{sl} \to 1$. For $R_{sl} > 1$ (tha is, for initially accelerating lenses) $C_{ch}(\infty)/f$ further drops (see Glaser, 1956)

The chromatic-aberration constant of unipotential lenses in dependenc on their geometrical data is demonstrated in Fig. 19. The minimum value o this aberration constant amounts to about three times the length of th

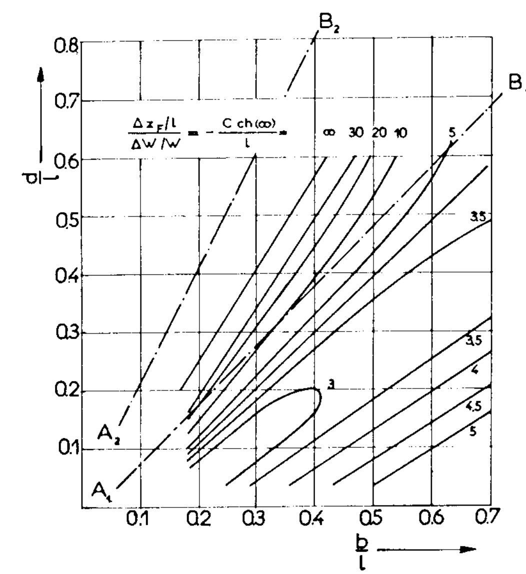

FIG. 19. The ratio of the chromatic aberration constant $C_{ch}(\infty)$ of symmetrical unipo tential lenses to the lens length l in dependence of the geometrical lens data accordin to Lippert and Pohlit (1953). Δz_F is the focal point displacement; $\Delta W/W$ the relativ energy shift; the other notations are as in Fig. 17.

lenses. For a lens with minimum aberration, the dislocation of the focal point amounts therefore to 3% of the lens length, if the energy shift of the particles amounts to 1%. At the telescopic operating point, the ratio of focal-point displacement to energy shifting becomes infinite. In weak lenses (that is, first operating range and focal points beyond the lens field) that have the same focal-point position, the chromatic aberration of the focal point is nearly independent of the lens geometries. Relativistic effects scarcely influence the chromatic aberration (Laplume, 1947).

d. *Distortion.* According to (27) and to Fig. 5, the distortion $\Delta Y/Y_0$ at a large distance behind the lens depends only on $\Delta f^*/f$, at which $\Delta f^* = f^* - f$, and f^* is equal to the focal length f for $\alpha' \to 0$ or $y \to 0$. Figure 20 demonstrates the dependence of $1/f^*$ on the angle of incidence α or on the height of incidence y; the $1/f^*$ characteristic can be obtained in the first approximation by displacing the lens power characteristic (compare Figs. 11–16) towards increasing values of R_{sl}. These displacements are very small and augment with increasing α or y. (The lens focuses "stronger" in the off-axis zones.) From this we recognize that within the direct vicinity of the power maximum, $1/f^*$ remains equal to the lens power $1/f$ for finite but small α or y. Hence the distortion vanishes at this point. (An example for application:

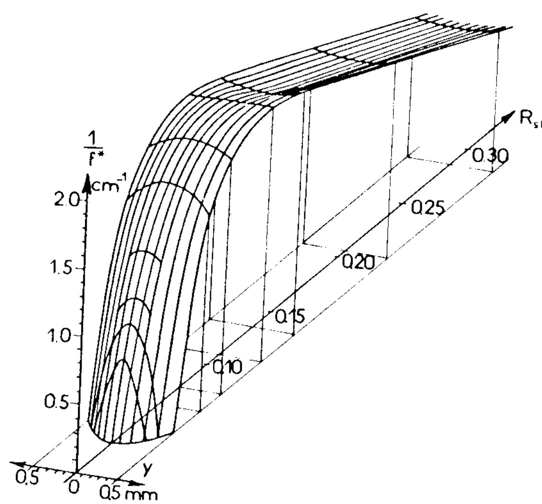

FIG. 20. Characteristic of the function $1/f^*(R_{sl})$ for the lens represented at the top of Fig. 2 (Heise, 1949). The principal point characteristic of this lens is shown in Fig. 9. y is the height of incidence. For $y = 0$, the characteristic is identical with the lens power characteristic.

the distortion-free projective lens, see Section 2.2.2,A,5b). For operating points with more positive values of R_{sl}, cushion-shaped distortion occurs and with more negative R_{sl}, barrel-shaped distortion occurs; for the second operating range the corresponding statements are valid.

As to the distortion of asymmetrical lenses, see 2.2.2,A,2f.

Numerical values for the distortion constant $c_d = -\Delta f^*/f\,\alpha'^2$ (see Eq. (42)] of *unipotential lenses* may be drawn from Fig. 21. Since the represented curves can be approximated mostly by straight lines, the distortion depends essentially on the ratio: thickness of the intermediate electrode to its bore diameter. We have to note that the distortion of weak lenses (that is, focal points beyond the lens field, cf. Figs. 17 and 18), which have the same z_F and f, severely depends on the lens geometry.

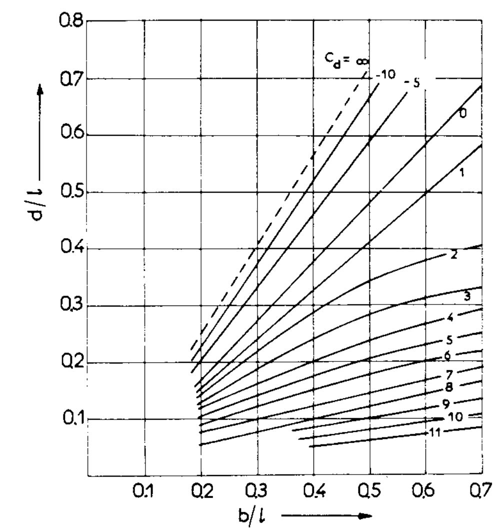

FIG. 21. The distortion of unipotential lenses in dependence of the geometrical data according to Lippert and Pohlit (1953). Notations are as in Fig. 17. Parameter is $c_d = \Delta Y/Y_0\,\alpha'^2$. $\Delta Y/Y_0$ is the relative distortion; α' the angle of emersion; positive sign of c_d indicates cushion-shaped distortion, negative sign of c_d barrel-shaped distortion.

e. *Spherical Aberration.* Mostly the values for spherical aberration are reported in the form $C_s(\infty)/f$. [$C_s(\infty)$ is the spherical-aberration constant related to the object for strong magnification (compare 2.2.1,A,5c)]. For the lens, known from the diagrams 2, 9, 20, Heise (1949) determined the minimum value $C_s(\infty)/f = 16$ at the maximum of the lens power ($R_{sl} = R_{sl\max}$). If the excitation of this lens is decreased ($R_{sl} > R_{sl\max}$) until the half-maximum power is reached, $C_s(\infty)/f$ raises to its double value.

If the lens excitation is increased ($R_{sl} < R_{sl\max}$) until the half-maximum power is reached, $C_s(\infty)/f$ raises to its 30-fold value.

As it was pointed out in Section 2.2.1,A,5c, the spherical aberration is completely determined by $\Delta z_{F'*}$, consequently, not by Δf^* alone. A graphical representation of the $z_{F'*}$ characteristic, from which the spherical aberration could be drawn in a similar manner like the distortion from Fig. 20, is not known. The spherical aberration has always the same sign, whereas the distortion is able to assume positive or negative sign (see Fig. 21). Rays, emerging from the object in greater angles, intersect the axis always at smaller distances behind the lens than the paraxial ones.

According to a rough rule, $C_s(\infty)/f$ has the order of 10 for initially decelerating single lenses, the focal points of which lie beyond the field.

Initially accelerating lenses have lower spherical aberrations. The spherical-aberration constants of *unipotential lenses* can be drawn from Fig. 22, which shows, in comparison with Fig. 19, that the spherical-aberration minimum nearly coincides with the minimum of the chromatic aberration and appears at operating points with voltage ratios something more positive than $R_{sl\max}$.

The spherical aberration of weak lenses (focal points beyond the lens field; compare Fig. 22 with Figs. 17 and 18) with the same focal point position depends only slightly on the lens geometry, and the spherical aberration of

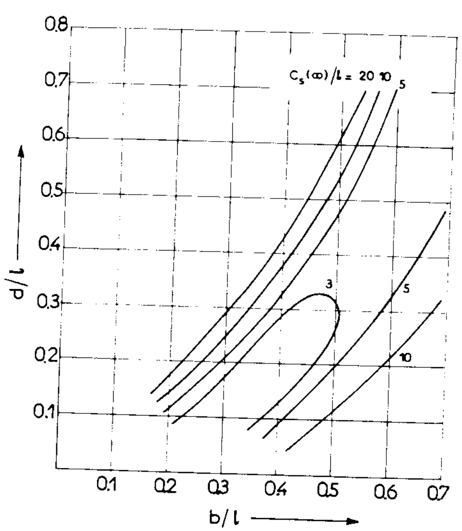

FIG. 22. Ratio of the "spherical-aberration constant $C_s(\infty)$ for strong magnification" to the "length l of the lens" in dependence of the geometrical lens data. Notations are as in Fig. 17 (Lippert and Pohlit, 1953).

weak lenses with the same focal length depends but scarcely on the lens geometry. According to Laplume (1947) the influence of relativistic effects on the spherical aberration of unipotential lenses is but inferior. For strong magnification, asymmetrical lenses have smaller or larger spherical aberrations than the corresponding symmetrical lenses, if the beam incides on the lens side with the higher or lower potential gradient, respectively (Hanszen, 1958b); compare to this, Section 2.2.2,A,2f and Fig. 26 (see furthermore, Seeliger, 1948). Septier (1959, 1960) utilized an asymmetrical lens with $C_s(\infty)/f = 2$ behind the ion source of a linear accelerator for protons.

Whereas it is mostly sufficient to know the relative spherical-aberration constant, the knowledge of the absolute value of the spherical-aberration constant is necessary for the determination of the electron-microscopical resolving power. The smallest distance ε, which can be resolved by transmission microscopes, depends on the wavelength λ of the electrons in the rays and on the spherical-aberration constant according to the equation, $\varepsilon \approx \approx (C_s(\infty)\lambda^3)^{1/4}$. Since, for electrostatic lenses used as objectives, the focal point always has to be located out of the lens field (see 2.2.2,A,5a), the spherical-aberration constant of usual electrostatic objectives (symmetrical unipotential lenses) has the large value of $C_s(\infty) = 60$ mm (see Seeliger, 1948). Only by very asymmetrical shaping of the intermediate electrode, Seeliger 1948 succeeded in reducing $C_s(\infty)$ to 23.5 mm. Compared with this, the spherical-aberration constants of the objectives currently used in the high-resolution magnetic microscopes amount to only 4 mm or less.

f. *Trajectories in the Off-Axis Lens Zones.* Figure 23 states, in which manner the slope of the exit asymptotes of a nearly parallel incident beam depends on the angle of incidence (or on the height of incidence); Fig. 24 shows the dependence of the axis intersection point on the same parameters. Under these circumstances $\Delta p' = \Delta z_{F'*}$. From the course of the represented curves for tan $\alpha \to 0$ or $y \to 0$, we can determine the cardinal elements (see Section 2.2.1,A,6b), and for small α or y the geometrical aberrations of the Seidel area (see Section 2.2.1,A,6c). The main advantage of these diagrams is to give the aberrations up to the outermost lens zones, without being tied to an approximate aberration theory.

Of particular interest is the knowledge of that lens zone which focuses parallel incident rays at a given distance behind the lens (that is we ask for details about the caustic). If we are concerned with an observation plane at the far distance s' behind the lens, in this plane the coordinate Y_i of a ray with the incident height y_i is only determined by the dependence of the emersion angle α_i' on y_i (see Fig. 4b). This holds because $\Delta p_i' \ll s'$.

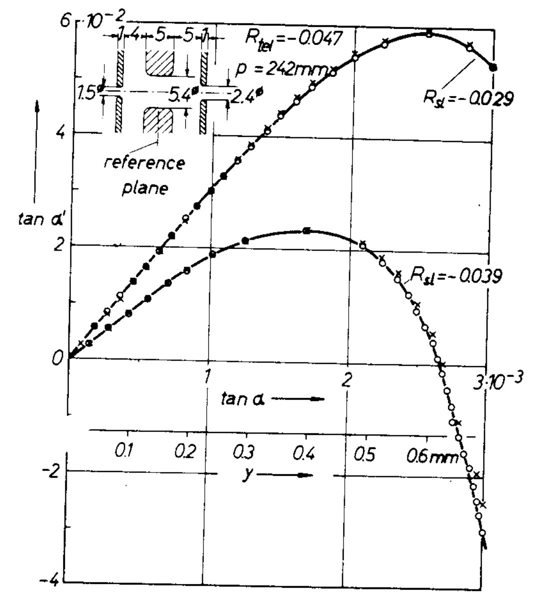

FIG. 23. Slope tan α' of the exit ray, emerging from an electrostatical single lens (similar to the lens of Fig. 16) in dependence of the slope tan α of the incident ray, or the height of incidence y, for different voltage ratios R_{sl} (Hanszen, 1964a).

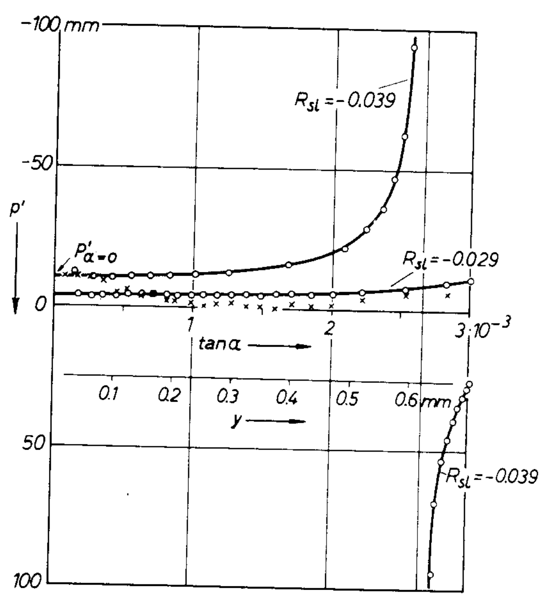

FIG. 24. Axis intersection points p' of the same lens as shown in Fig. 23 for two different voltage ratios. Notations as in Fig. 23.

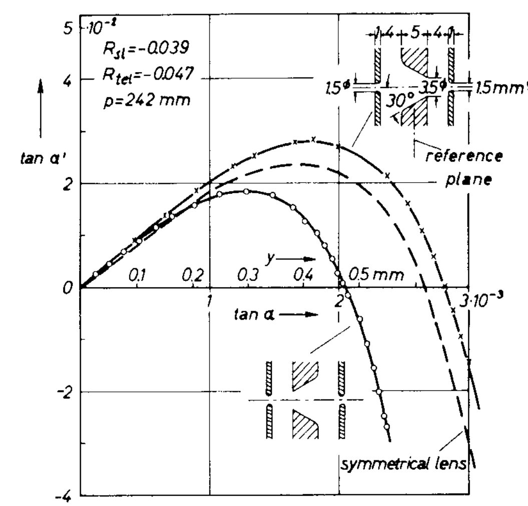

FIG. 25. Confrontation of the slope tan α' of the exit rays emerging from symmetrical and asymmetrical single lenses. The beam enters the lens nearly parallely to the axis from the *left-hand* side. Notations are as in Fig. 23 (Hanszen, 1958b).

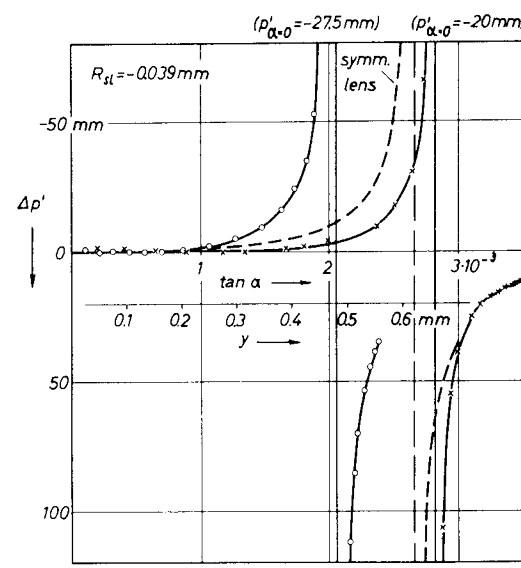

FIG. 26. Confrontation of the longitudinal spherical aberration of the symmetrical and asymmetrical single lenses shown in Fig. 25. Notations are as in Fig. 23 (Hanszen, 1958b).

Therefore, the intersection of the caustic with the observation plane (this means, Y_i to be independent of α_i or y_i) is determined by the maxima of the curves shown in Fig. 23. Hence, the focusing lens zone can immediately be determined from this figure. The dependence of the curve tan $\alpha'(y)$ on the voltage ratio supplies information about the "chromatic aberration of the distortion," since in accordance to (46) the R_{sl} dependence can be converted into a W dependence. This aberration causes the *energy dispersion* of energy analyzers. Details about focusing and analyzing properties of electrostatic lenses are given in 2.2.2,A,5c.

The data of the rays in the off-axis zones of *asymmetrical single lenses* can be drawn from Figs. 25 and 26. According to the direction of the parallel incident beam, the longitudinal *spherical aberration* is larger or smaller than the aberration of the corresponding symmetrical lenses, the higher potential gradient being located at the entrance or exit side of the lens, respectively. For small α or y, the course of the curves shown in Fig. 26 gives according to (38) and (40) the "spherical aberration constant for strong magnification" in the inversed ray tracing. (These measurements are, however, of low accuracy.)

For small α or y, the course of the curve shown in Fig. 25 determines the focal length of the lens [see (43)]. Since both focal lengths of asymmetrical single lenses are equal, the curves belonging to both lens positions must have the same slope at the origin of the coordinate system. Because of the result given in Fig. 16, however, this slope is larger than that of the curve belonging to the corresponding symmetrical lens. This slope and further details about the trajectories in the external zones of the symmetrical lens can be drawn from Fig. 23.

3. *Gauze Lenses as Single Lenses*

The general properties of these lenses have already been reported in Section 2.2.2,A,1. Of particular interest are the voltage ratios $R_{sl} > 1$ (the incident particles are initially accelerated) at which the gauze lenses work as converging lenses. According to Fig. 27, the lens power $1/f$ equals to 0 for $R_{sl} = 1$ and increases linearly with $(R_{sl} - 1)$. For this reason, with R_{sl} somewhat above 1, the lens power is considerably stronger than the power of an ordinary three-diaphragm lens, the power of which increases proportional to $(R_{sl} - 1)^2$. Hence gauze lenses may always be utilized where particles with very high energies have to be focused by the aid of limited lens voltages (for example, in linear accelerators for ions. For data on gauze lenses as accelerating lenses see Section 2.2.2,B,1).

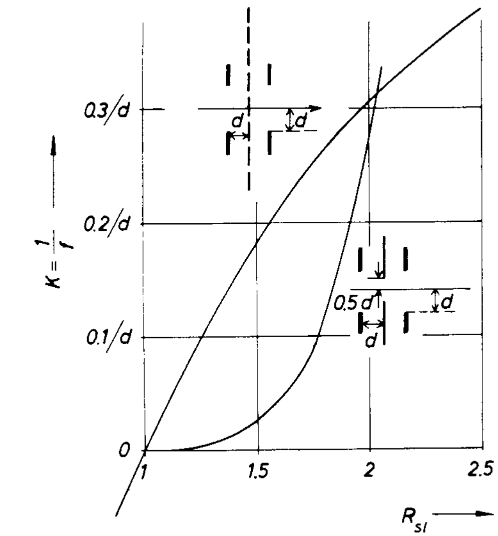

FIG. 27. Lens-power characteristic of a gauze lens compared to the characteristic of the corresponding three-diaphragm single lens with very thin electrodes and for an initially accelerating field between entrance and intermediate electrode ($R_{sl} > 1$) (Bernard, 1953a).

The geometrical aberration of gauze lenses are smaller than the aberrations of the corresponding three diaphragm lenses. According to Bernard (1952), the spherical aberration of diverging gauze lenses can even get negative values. Also the other aberrations of these lenses are so small that they appear suited for the imaging of extended object fields (Verster, 1963).

Mostly electroplated gauzes are utilized as gauze electrodes. At present they can be manufactured with a minimum lattice constant of 12.5 μm (and with a transparency of about 70%). Each mesh of the gauze has a weak diverging effect in converging lenses and a weak converging effect in diverging lenses. These effects limit the resolving power of the gauze lenses more than the spherical aberration. The smallest resolved distance is somewhat smaller than the grating constant of the used gauze (Bernard, 1953b).

4. *Three-Tube Lenses*

Three tube lenses are scarcely used for imaging purposes but frequently for the collecting of beams with high divergence. These lenses mostly consist of three coaxial tubes of equal diameter with short mutual distance apart. Even tubes with diameters up to some decimeters are in use. Their lens properties can be reduced from those of three diaphragm lenses with small electrode distances and large electrode thicknesses (for example, from Fig. 17 with $d/l \to 1$). According to Liebmann (1949) the focal length of unipotential lenses consisting of tubes with the diameter $b \geqq d + a$ is given by the rule of thumb,

$$f = b^2/(d + a) \tag{50}$$

where d is the length of the intermediate tube and a the distance between two tubes.

Liebmann (1949) and Gobrecht (1941) reported further details about these systems for the Gaussian and the Seidel area. Lens-power maxima occur with these lenses too. For the spherical-aberration constant of unipotential lenses it yields approximately:

$$C_s(\infty)/f = 10(f/b)^2 \tag{51}$$

5. *Examples for the Application of Electrostatic Lenses*

a. *Electrostatic Lens as the Objective of a Microscope.* Because a very strong magnification is required in the microscope, the object must be located close to the first focal point of the objective. Therefore, we are allowed to use only lenses with focal points outside the field because the object is not permitted to disturb the lens field. Since for objective lenses, customary symmetrical unipotential lenses are in use, according to Fig. 22 in connection with Figs. 17 and 18, we have to reckon with spherical-aberration constants $C_s(\infty)$ not remarkably below 10 lenses lengths. Since for an operating point with minimum spherical aberration the focal point is always located within the lens field, it is not possible to take any advantage of this operating point for objective lenses. For the operating point with minimum chromatic aberration, the same statement is valid. These are serious disadvantages of the electrostatic objectives contrary to magnetic objectives, since for the latter the object is generally allowed to dip into the magnetic field. To assure a satisfactory breakdown rigidity (see Section 2.2.3,B), the electrodes have to be arranged with sufficient interspaces. This requirement prohibits production by electrostatic lenses of focal lengths as small as those produced by magnetic lenses. According to Seeliger (1948), the focal lengths of the common electrostatic objectives are 6–7 mm. Magnetic objectives however have focal lengths of 2 mm or less.

b. *The Electrostatic Projective Lens.* The image generated by the objective lens acts as object for the projective lens. This image of course is allowed to dip into the projective field. Therefore, this lens can be operated

at its power maximum and it is possible to generate a distortion free image see Section 2.2.2,A,2d. (Strictly speaking the osculatory cardinal points are competent instead of the virtual ones for this imaging purpose.)

c. *Electrostatic Lens as Energy Analyzer.* In the energy analyzer, the particles of an parallel incident beam with finite energy width will be separated according to their energies. Simultaneously, the particles with equal energy will be focused in the recording plane. The separation is done by the "chromatic dependence of the distortion" in the external zones of the lens. This dependence can be derived from the family of curves, drawn in Figs. 23 and 28, considering the fact, that the relative energy deviation $\Delta W/W$ of the particles is coupled with the voltage ratio according to (46). The focusing is realized according to Möllenstedt and Dietrich (1955) and Dietrich (1958) in the caustic ray tracing, that is, by applying the lens zones, for which the curves of Fig. 23 have their maximum values. Unfortu-

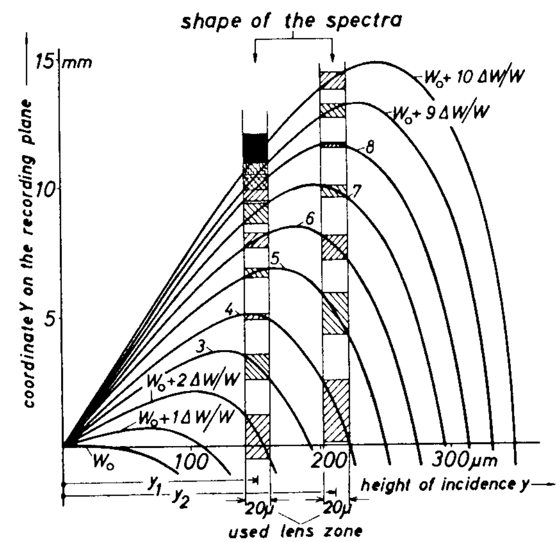

FIG. 28. Design of an energy spectrum $W = W_0 + n\,\Delta W/W$ (equidistant spectral lines) if two lens zones with different heights of incidence y_1 and y_2 are utilized (schematic)

nately, this condition is only fulfilled for one single energy, so that we have exact focusing only for one single spectral line. These facts are demonstrated in Fig. 28.

The slope, and especially the radius of curvature at the extrema of the curves are decisive for the admissible latitude of the lens zone which can be utilized and on that account also for the *transmission* of the spectrometer. The rise between the maxima of two adjacent curves is decisive for the dispersion of the spectrometer. The run between the maxima of two adjacent curves is decisive for the unsharpness of the spectral lines not exactly focused; hence it determines the *defocusing*. The properties of each lens are described by a family of curves like Figs. 23 and 28. The families belonging to every possible lens approximately can be deduced from one another by suitable linear but generally *independent* transformations *of both coordinates* (see Lippert, 1955b). Lenses with thin intermediate electrodes generally have stronger dispersion, but also larger defocusing than lenses with thick intermediate electrodes.

To either side of an asymmetrical lens belongs a different diagram, similar to Fig. 28. One diagram results from the other with sufficient accuracy by *transformation of both coordinates* in an *equal scale*. [For example, proved for the asymmetrical lens of Fig. 15 by Hanszen (1956) published only as Congress report.] If the higher potential gradient lies on the exit side, the dispersion—and the defocusing too—rises in an equal ratio above the values belonging to the opposite ray tracing.

In order to be independent of voltage fluctuations, there are nearly always unipotential lenses in use for energy analyzing. Moreover, lenses with rotational symmetry are replaced by cylindrical lenses, for which the above statements are also valid (Metherell and Whelan, 1966).

There is a lack of detailed experimental material about cylindrical lenses; theoretical data are published by Archard (1954).

d. *Filter Lenses.* For filtering purposes we take advantage of the strong retarding effects in electrostatic lenses (Möllenstedt and Rang, 1951; Boersch, 1954; Lippert, 1955a; Hahn, 1959, 1961, 1964): Filter lenses for the electron miscroscopes are required to exclude all electrons with higher energy losses than 6 eV from the beam and to focus the electrons with energy losses of only some tenths of eV in order to form an image with the demanded resolution. On one hand, because of the minimum chromatic- and spherical-aberration values at the lens power's maximum, filter lenses should be operated at this maximum in order to have good imaging properties for the electrons without energy losses. On the other hand, to fulfill the filtering condition, it is indispensable for the saddle potential to approach the original rest potential within 6 V. Unfortunately this does not happen in the lenses at the first power maximum. Hence filter lenses give an example for the practical importance of higher order operating ranges. Since it is not possible for objectives to operate at a lens power's maximum, only

projectives or intermediate lenses may be used as filter lenses; according to Section 2.2.2,A,5b and under the above conditions, simultaneously the image is distortion free too. Filter lenses for microscopes generally have a very thin intermediate electrode with a very small bore.

Lenses with a narrow bore in a thick intermediate electrode are suitable for filter lenses in beams with big cross section, if only less demands on focusing quality and energy resolution are wanted (Deichsel and Keck, 1960). Long-focus filter lenses (practically operating with telescopic ray tracing) with large aperture can be realized by five-electrode systems (Simpson and Marton, 1961; Kessler and Lindner, 1964). An interesting filter lens with coupled electric and magnetic fields has been designed by Brack (1962) and Hartl (1966).

e. *Electron Mirror.* With increasing retarding potential at the intermediate electrode, first the off-axis lens zones and finally the axis area exceed the rest potential of the particles. Therefore, first the off-axis zones and then by degrees the whole lens acts as a mirror for particles with equal energy. The power of the mirror—like the power of lenses—has oscillatory sign in dependence on the potential of the intermediate electrode. For very strong reflecting potentials diverging mirrors result. Details and the description of specific systems can be drawn from Hottenroth (1937) and for two-tube mirrors from Nicoll (1938).

B. Immersion Lenses

"Immersion lenses" is the collective name for accelerating and decelerating lenses. Mostly these lenses consist of two electrodes. As significant voltage ratio we introduce the quantity

$$R_u = \frac{U' - U_0}{U - U_0} \tag{52}$$

where U_0 is the rest potential of the particles, U the potential of the electrode on the object side, and U' the potential of the electrode on the image side.

If the object and image spaces are field free, that is to say, if they have uniform potentials U and U', respectively, for the immersion lenses, we can introduce cardinal elements again. For nonrelativistic particle velocities the ratio of the focal lengths f and f' on the object and image side is given by

$$f/f' = \div [(U - U_0)/(U' - U_0)]^{1/2}; \tag{53}$$

the corresponding relation for the relativistic range can be easily deduced from (4) and (44).

The foregoing statements hold particularly for two-diaphragm and two-tube lenses, the properties of which shall be discussed in this article only in reference to gauze immersion lenses; details about two-electrode lenses will be described in Chapter 5.1 in connection with accelerators.

1. *Gauze Immersion Lenses*

Verster (1963) investigated two gauze immersion lenses, consisting of two coaxial tubes of equal diameter arranged with short distance apart, wherein the tube on the image side was equipped with a flat or convex gauze. The results of these measurements are represented in Figs. 29 and 30. The

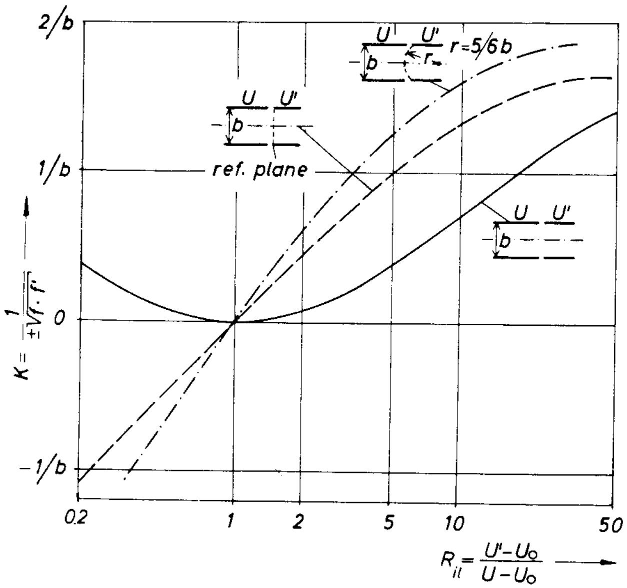

FIG. 29. Confrontation of the lens power characteristics of two gauze immersion lenses with the characteristic of the correspondent gauzeless two-tube immersion lens (according to Verster, 1963).

lens power characteristics of these lenses can be compared in Fig. 29 with the characteristic of a two-tube lens without gauze. Similarly as the gauze single lens described in Section 2.2.2,A,3 and Fig. 27, the gauze immersion lenses diverge the beam in the operating range with $R_{il} < 1$ and collect it with $R_{il} > 1$. For $R_{il} \approx 1$ their power increases proportional to (log R_{il}):

therefore, the absolute value of the power in this range greatly exceeds the power of a lens without gauze, which rises proportional to (log $R_{il})^2$. Thus, gauze immersion lenses can be utilized for the same purpose as gauze single lenses (see Section 2.2.2,A,3).

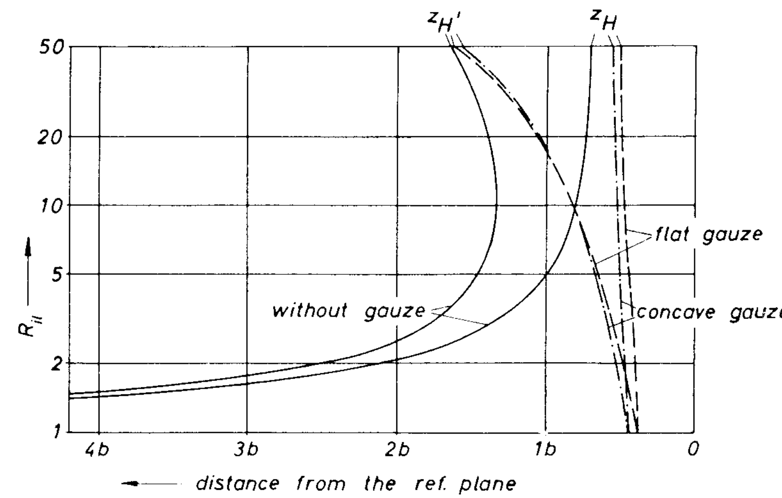

FIG. 30. Principal point characteristics of the lenses shown in Fig. 29 (Verster, 1963).

Figure 30 represents the principal point characteristics of both gauze immersion lenses. Whereas the principal planes of normal immersion lenses move toward $z = \infty$ on the object side for $R_{il} \to 1$, the principal points of gauze lenses remain at a finite distance.

Chromatic-aberration constant C_s, focal lengths f, f', and tube diameter b are connected by the following equation:

$$\text{Object on the side with the potential } U\text{: ... } C_s(\infty)/f = Aff'/b^2 \quad (54)$$

$$\text{Object on the side with the potential } U'\text{: ... } C_s'(\infty)/f' = A'ff'/b^2 \quad (55)$$

Herein, the quantities A and A' are nearly independent of R_{il} and scarcely differ from one another. For accelerating lenses without gauzes and for not too large R_{il}, $A \approx A' \approx 2.4$; for both gauzes lenses, shown in Fig. 29, under the same conditions, $A \approx A' \approx 1.9$. About further geometrical aberrations see Verster (1963). About the influence of the gauze meshes on the image quality see 2.2.2,A,3.

2. *The Single Aperture*

A *small* bore of the diameter b in a very thin diaphragm at the potential U leads to an inhomogeneity in the electrical *fields* in the halfspaces on both sides of the diaphragm. The original fields may have the field strengths E and E' and may be directed perpendicularly to the diaphragm plane. Then the inhomogeneity focuses a parallel beam of particles at the distance $z_{F'*}$ on the image side (counting the axis coordinate in the beam direction!):

$$z_{F'*} = \frac{4\,(U - U_0)}{E - E'} \tag{56}$$

where $W = e(U_0 - U)$ is the energy of the particles, when passing the diaphragm plane.

The single aperture acts as *diverging lens*, when the acceleration decreases or the deceleration increases for particles moving from the field E into the field E'; that is:

(a) for accelerating fields on both sides (E; $E' < 0$ for negative particles and E; $E' > 0$ for positive particles) with $|E| > |E'|$;

(b) for decelerating fields on both sides (E; $E' > 0$ for negative particles and E; $E' < 0$ for positive particles) with $|E| < |E'|$;

(c) for an accelerating field on the incidence side and decelerating field on the exit side ($E < 0$; $E' > 0$ for negative particles and $E > 0$; $E' < 0$ for positive particles) with arbitrary amounts of E; E'.

In all other cases the aperture acts as *converging lens*.

Particularities about the influence of the diaphragm thickness are published by MacNaughton (1952), about the influence of the bore diameter by Hoeft (1959).

If the fields have opposite directions in both halfspaces and the field on the incidence side is a decelerating one, the saddle potential in the bore of the diaphragm may assume such a height, that the particles no longer are allowed to pass the aperture. If the decelerating field decreases, the potential barrier opens for the beam in the manner of an iris. (Application: grid-electrode in electron guns).

3. *Immersion Objective Lens for Electron Microscopes*

The immersion objective consists

(a) of an emitting plane cathode surface, whose potential can be identified, without a large error, with the rest potential U_0 of the particles;

(b) of a single aperture at the potential U as grid electrode; and

(c) of a single aperture at the potential U' as anode.

Consequently, the object is a part of the lens, and the lens properties depend strongly on its position. Because the object space is not field free, it is not possible to determine image position and magnification by means of cardinal elements according to (2).

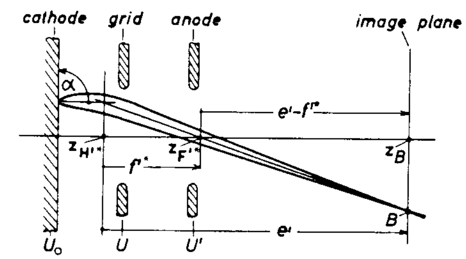

FIG. 31. Ray path of an elementary bundle in an immersion objective (schematic).

In most cases, we are allowed to assume the field just in front of the cathode to be homogeneous and axially directed. The electrons emitted from each element of the cathode into the angle $2\alpha = \pi$, in this case, are bundled into a narrow elementary beam with a chief ray initially parallel to the axis (see Fig. 31). The field, generated by grid electrode and anode, focuses the elementary beam into the image element B. The tangent line to the chief ray in the image point B intersects

(a) the axis at the point $z_{F'*}$ and

(b) the tangent line to the chief ray in the object point, at the point with the z coordinate $z_{H'*}$. With the quantities f'^* and e' (the meaning of which can be seen on the figure) the magnification can be expressed by

$$M' = -\,(e' - f'^*)/f'^* \tag{57}$$

Hence, image position and magnification are known, if $z_{H'*}$, $z_{F'*}$ and the coordinate z_B of the image plane are known as a function of the geometrical parameters (essentially electrode distances, thickness and bore diameter of the grid electrode) and the voltage ratio. The manner in which M' and f'^* depend on the geometrical data, if the image plane has a fixed position at a large distance from the lens, is examined in great detail by Septier (1954a). Beyond that, Soa (1959) published systematic investigations for other image distances. The example, given in Fig. 32, permits to compare the course of $z_{H'*}$, $z_{F'*}$, z_B with the course of the cardinal elements of single lenses (see for example, Fig. 9); but it must be emphasized that for immersion lenses an object displacement (that is, a cathode displacement) will involve an alteration of the whole characteristic. Soa (1959) proved the

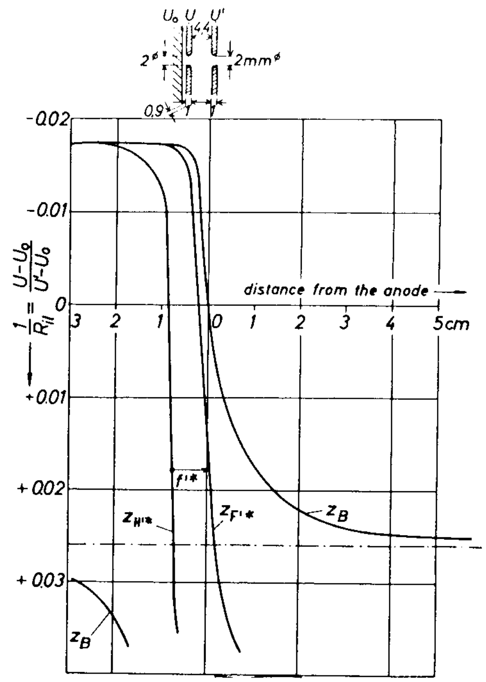

FIG. 32. Characteristic of an immersion objective. z_B is the image coordinate; $z_{F'}*$ the axis intersection of the chief ray's asymptote on the image side; and $z_{H'}*$ the axis coordinate of the intersection point between the two asymptotes of the chief rays on the object and image side (Soa, 1959).

quantity $1/f'^*$ to pass a maximum value in dependence on the voltage ratio R_{il} (see Fig. 33) as it is known for the lens power of single lenses. His supposition that the imaging qualities of immersion objectives improve if the operating point approaches to this maximum could be confirmed by experiments. According to the published figures, especially the field curvature and the off-axial astigmatism [more about these errors can be read in Septier (1954a)] decrease when approaching to the maximum. But unfortunately it is not possible to reach this maximum with strong magnifications (that is, with large image distances). In order to raise $1/f'^*$ toward its maximum value, we are compelled to make the grid electrode thin, its

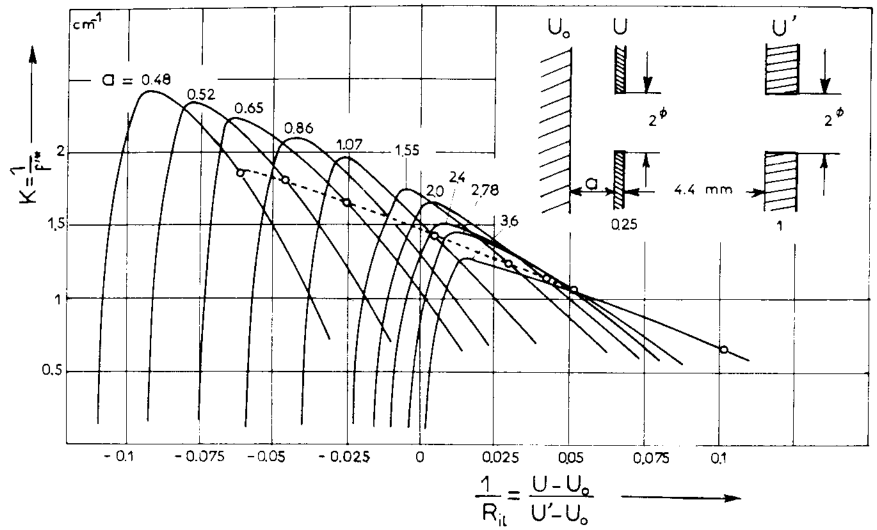

FIG. 33. The $1/f'^*$ characteristics of an immersion objective in dependence on the distance between cathode and grid electrode (Soa, 1959). The dotted line refers to image positions $z_B \to \infty$.

bore as large as possible and the distance between grid electrode and anode small (with this compare Bas and Preuss, 1964).

But under these circumstances no extreme resolution power is attainable. According to the geometric–optical consideration of Recknagel (1941); [compare the synopsis given by Septier (1954b)], the minimum resolved point distance (gained without applying an aperture stop) approximately amounts to $2kT/eE$ independent of the specific field distribution. (kT is the half-energy width of the emitted electrons and E the field strength in front of the cathode.) This expression, which still calls for a wave mechanical correction (Recknagel, 1943), in the most cases has been experimentally proved to be sufficient for high field strengths. According to these results, the resolving power increases with the cathode field strength. The relatively low resolution of the previously discussed lens therefore is caused by the weak cathode field strength. While maintaining a fixed *large image distance*, the field-strength cannot be raised by diminishing the distance between cathode and grid, because the required variation of the grid potential counteracts this raise. Only the bore diameters of the two diaphragms have influence on the field strength. Satisfactory values of the field strengths and the possibility to operate at the maximum of $1/f'^*$ only can be expected, according to Soa (1959), for small image distances, that is, for weak magnifications. According to the statements of Septier (1954a) the value for the cathode field strength (measured in kV/cm) of the classical immersion lenses has the 0.5 to 0.8-fold numerical value of the accelerating voltage (measured in kV). In order to realize higher field strengths at the cathode, Septier (1954a) proposed (besides alterations of the electrode shapes) to separate the accelerating and the imaging field; that is, to annex a *single lens* to the accelerating field. In the experiments to this proposal, the aberrations of the imaging field however surpassed the aberrations of the accelerating field. Only in the last time, Illenberger (1964) succeeded in obtaining highly resolved and distortion free images by utilizing a single lens with an extremely small bore in a thin entrance electrode.

The electrostatic imaging field of this immersion objective also can be replaced by a magnetic lens.

It is possible, to improve the resolution of all immersion objectives about 3 to 4 times by using an aperture stop. Instructive micrographs for the influence of the aperture stop are shown by Bayh (1958).

For theoretical investigation of the immersion objective see Hahn (1958).

4. *The Electron Gun as Immersion Lens*[3]

In electron guns too, the electrons emitted from the cathode, must be accelerated and focused. But contrary to the purpose to be fulfilled with immersion objectives, electron guns are not intended to image the cathode surface, but instead to transfer as many electrons as possible through a pupil cross section (crossover) as small as possible, located at the fixed distance $z_{F'*}$ (see Fig. 31).

Generally, the cathode surface is curved. In the simplest case of rotational symmetry the cathode has the shape of a spherical cap. Such a system has strong geometrical aberrations. The chief rays of the elementary bundles, starting from all elements of the cathode surface, intersect by no means at one single point, but they form an intricate caustic (Hanszen, 1962) whose shape can be exactly determined by the aid of the shadow method (Hanszen, 1964a). In this way, complicated intensity distributions over the beam cross section, especially in the so-called "hollow beams," are surveyed easily. In the course of these investigations it could be shown (Hanszen, 1964b,c), that even at the normal operating point of electron guns, a unitary crossover may not be present. The conditions for a point-focus or a cone-focus at a large distance from the cathode can be determined also by this shadow method. A special contribution in this book, see Chapter 2.1, is dedicated to the specific properties of electron guns.

[3] Compare also the recent publications of Lauer and Hanszen (1966) and Lauer (1967).

C. Electrostatic Stigmators (Correction of Axial Astigmatism)

Because of the mechanical tolerances, the shape of all electrostatic lenses departs, more or less, from an exact rotational symmetry; *axial astigmatism* results from this. External disturbances (such as electrical charges on the glass windows and insulators, the magnetic-earth field, contaminations on the electrodes, and so on) act in a similar manner. As far as the astigmatism originates from the single parts of the lens, it is possible to compensate the astigmatism components of the different lens parts by turning them around the axis against each other (see for example, Hahn, 1954).

Over and above this, it is possible to compensate the residual astigmatism —it is nearly always binary—by a cylindrical lens, that is, a so-called stigmator. In the simplest case, it can be realized by a single lens with a slot-shaped aperture in the intermediate electrode. This lens has to be located at an appropriate place of the ray path, and its strength has to be adjusted by varying the potential of the intermediate electrode.

A quadrupole lens serves for the same purposes. Since an azimuthal mechanical turning of the stigmator lens under vacuum conditions cannot easily be realized, an electrical turning is often preferred. To enable this, according to Rang (1949), two quadrupole lenses, which are composed of a system with "octopole-like" geometry, are used. By proper regulation of the excitation of both quadrupoles, it is even possible to choose direction and amount of the compensating astigmatism independent from one another.

2.2.3. Practical Aspects for the Construction of Electrostatic Lenses

A. Mechanical Tolerances, Shielding of Stray Fields, Highest Admitted Voltages

During the construction of electron lenses, exact rotational symmetry of all field influencing components must be observed. For example, in electron microscopes the noncircularity of each electrode bore and the deviation of their centers from a concentric position should be less than 1/100 mm. The lens chamber should be made of soft iron in order to shield external —particularly alternating—magnetic fields. For extraordinary cases, an additional "Mu-Metal" shielding may be used. Good materials for the insulator between high-voltage supply line and lens-chamber are nonporous ceramics or synthetics like "acryl-glass" and "epoxy-resin," which can be worked easily on a lathe. Size and shape of the insulator are guided by the applied voltage (see Figs. 36, 37). Mostly, the point of the question is to obtain strong lens powers. Therefore, we need a very high field strength between the lens electrodes. For this reason the designing of the electrode system including the insulators between the electrodes is closely referred to the problem of breakdown rigidity. Particular details in the design of these lens elements are given in the following chapter in connection with the discussion of the breakdown rigidity. As known by experience, it is possible to maintain the following field strength between the lens electrodes:

approx. 100 kV/cm without greater difficulty;
approx. 150 kV/cm with careful design of the components;
approx. 200 kV/cm only with best design and meticulous cleanness.

These facts will be illustrated by an example: The focal lengths, needed in the electron microscopy, are smaller than 1 cm. According to the statements of 2.2.2,A,5a and Figs. 17, 18, the realization of the foregoing objective focal length requires an electrode distance smaller than the focal length itself. For this reason, and with the fore-mentioned breakdown field strengths, we can hardly maintain higher voltages than 60 kV between the lens electrodes. For the same reason, it is not possible to design electrostatic lenses with focal lengths remarkably below 1 cm for particle energies higher than 60 keV.

B. Breakdown Rigidity of the System "Lens-Electrodes and Insulator"

Just before reaching the breakdown-voltage, the so-called "microdischarges" occur (Arnal, 1955). They are induced by cascades of positive and negative ions and electrons that release each other by impact from the contamination layers on the electrodes (Boersch *et al.*, 1961; 1966; Arnal and Bouvier, 1965). They are extinguished if the voltage is lessened by approximately 1 kV; (facility: resistance in the feed line). If a protective resistance of 50 MΩ is used, the voltage dip endures only 10^{-4} sec. But even then, the microdischarges disturb the operation of electron-optical apparatus severely (see Boersch *et al.*, 1961). Some causes for microdischarges and some methods on how to avoid them are discussed in the following sections.

When the discharge current increases, electrode material is evaporated and sparkovers with complete voltage breakdowns occur. The evaporation of electrode material can be reduced with the aid of the above-mentioned protective resistance; for in that case, the charge transported by one spark

is only determined by the capacitance of the lens system which, for this reason, should be as small as possible (Rabinowitz, 1965).

1. *Microdischarges between Two Electrodes*

Microdischarges are released by electrons which are emitted from very small protrusions on the negative electrode by field emission (Chatterton, 1966). Provided that the electrodes are covered with a thin insulating layer of hydrocarbons (such as oil from vacuum pumps), field emissions occurs already at a field strength of 10^4 V/cm, independent of the cathode material, if the contamination layer is polarized by the impinging of positive ions ("Malter-Effect", see for example, von Ardenne, 1956; Boersch *et al.*, 1964). The way, in which the released discharges run off, however, depends on the anode material and the quantity of adsorbed hydrogen (Arnal, 1955). The rush of the microdischarge current leads to sudden evaporation of the cathode protrusions and thus to sparkover formation (Davies and Biondi, 1966).

A convenient anode material is stainless steel; for laboratory experiments duralumin often suffices (Gölz, 1940). The breakdown rigidity is raised by rounding off the edges and polishing the surfaces of electrodes. Moreover, it is advantageous to confine the area of highest field strength to these parts of the field which are important in leading the beam. Curved electrode surfaces are of advantage (Miller, 1966). The electrodes have to be cleaned by polishing; in critical cases the hydrocarbons must be cracked by heating or by glow-discharge at a pressure of 10^{-1} to 1 Torr. Residual emissions centers may be destroyed by arbitrary produced flashes with limited current. The breakdown rigidity is raised by a very small leak in the vacuum chamber near the critical electrodes (Schumacher, 1966). As shown by Arnal (1955), the geometry of the electrodes should be designed in such a way that flashes are not allowed to strike the insulator and to form contamination layers on its surface.

2. *Microdischarges on the Insulator Surface*

As is known from experience, the junction between negative metal and dielectric is a source of electrons and therefore a starting point of flashovers. The electron emission increases with the permittivity of the insulator material, and is nearly independent of the electrode materials (Kofoid, 1960a). Further details are reported in Grivet's textbook (1958). The electron emission can be suppressed by reducing the field strength at the junction.

This can be done by suitable geometrical design (see Fig. 34) and by using an insulator material with low permittivity (Kofoid, 1960b).

Beyond this, a positive charge on the insulator surface, caused by secondary emission of electrons, must be avoided. According to Boersch *et al.*

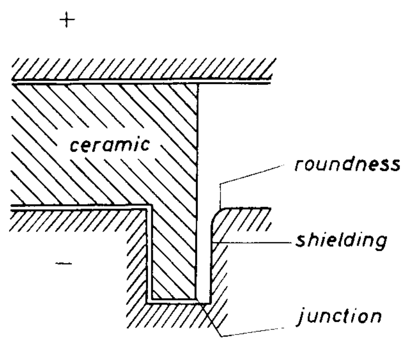

FIG. 34. Design of the junction between insulator and negative electrode. The electron emission is suppressed by lowering the field strength at this place. This can be done by "electrostatic shielding" of the junction and by rounding off the electrode edges (Kofoid, 1960b).

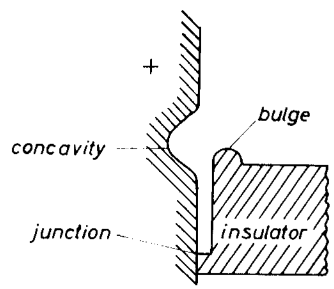

FIG. 35. Design of the junction between the insulator and the positive metal chamber of an electron lens (Gribi *et al.*, 1959). The concavity in the chamber wall reduces the field strength. By this shaping and the insulators' bulge, it is avoided that the electrons are stripped off from the negatively charged insulator.

(1963), by choosing a proper angle between insulator surface and field direction, it is principally possible to gain an uncharged or only negatively charged insulator surface near the junction. If such an angle cannot be realized, the distance between negative electrode and point of impact of the electrons on the insulator should be so large that a sufficiently high-po-

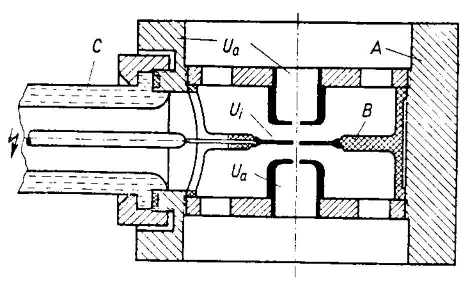

FIG. 36. Electron single lens for the electron-optical bench designed by Boersch (1951); see also Boersch (1940) and Mahl (1940). *A* is the lens chamber, consisting of iron or aluminium; *B* the high-voltage insulator, consisting, for example, of hard rubber (ebonite); and *C* the insulator for the high-voltage supply line, consisting of acrylglass.

tential difference occurs. Then, the electrons striking the insulator have energies high enough so that the secondary emission factor falls below 1. Under these circumstances, the insulator surface is only enabled to keep negative charge or none. Thus, the noxious field strength between insulator and cathode is diminished. A negative charge of the insulator raises however the potential difference near the positive electrode and may possibly lead to a stripping off of electrons from the insulator's surface. This effect can also be avoided by suitable geometrical design of the insulator and the positive electrode, see Fig. 35.

C. Examples for Design

Figure 36 represents a single lens, designed for laboratory devices; Fig. 37 shows an objective-lens, which especially is flashproof and which is used in commercial electron microscopes. Further proposals for designing may be taken out of the tabular compilation by von Ardenne (1964).

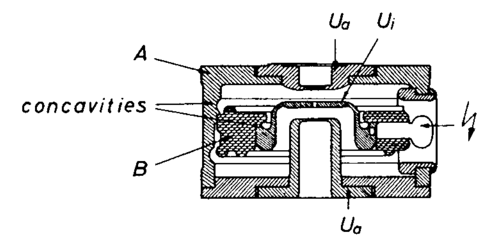

FIG. 37. Objective lens of a 70-kV microscope (Gribi *et al.*, 1959). *B* is the insulator, consisting of a mixture of epoxy-resin and quartz. (For less demanding purposes an epoxy-resin and talcum mixture is sufficient). All junctions metal-to-insulator are located at places with low field strength. According to the junction insulator B to lens chamber A compare to Fig. 34.

REFERENCES

Archard, G. D. (1954). *Brit. J. Appl. Phys.* **5**, 179 and 395.
Archard, G. D. (1956). *Brit. J. Appl. Phys.* **7**, 330.
Arnal, R. (1955). *Ann. Phys. (Paris)* [12] **10**, 830.
Arnal, R., and Bouvier, P. (1965). *Compt. Rend.* **260**, 4944.
Bass, E. B., and Preuss, L. (1964). *Optik* **21**, 261.
Bayh, W. (1958). *Z. Physik* **151**, 281.
Bernard, M. Y. (1952). *Compt. Rend.* **235**, 1115.
Bernard, M. Y. (1953a). *J. Phys. Radium* [8] **14**, 381.
Bernard, M. Y. (1953b). *J. Phys. Radium* [8] **14**, 451.
Boersch, H. (1940). *Jahrb. AEG Forsch.* **7**, 34.
Boersch, H. (1951). *Z. Physik* **130**, 517.

Boersch, H. (1953). *Z. Physik* **134**, 156.

Boersch, H., Hamisch, H., and Wiesner, S. (1961). *Z. Angew. Phys.* **13**, 450.

Boersch, H., Hamisch, H., and Ehrlich, W. (1963). *Z. Angew. Phys.* **15**, 518.

Boersch, H., Hamisch, H., and Markmann, G. (1964). Proc. Int. Symp. on Insulation of High Voltages in Vacuum, Cambridge (Mass.), p. 113.

Boersch, H., Hamisch, H., and Schirrmeister, H. (1966). *Z. Angew. Phys.* **22**, 5.

Brack, K. (1962). *Z. Naturforsch.* **17a**, 1066.

Chatterton, P. A. (1966). *Proc. Phys. Soc.* (London) **88**, 231.

Davies, D. K., and Biondi, M. A. (1966). *J. Appl. Phys.* **37**, 2969.

Deichsel, H., and Keck, K. (1960). *Optik* **17**, 401.

Dietrich, W. (1958). *Z. Physik* **151**, 519.

Everitt, C. W., and Hanszen, K.-J. (1956). *Optik* **13**, 385.

Felici, N. J. (1959). *J. Phys. Radium* [8] **20**, 97 A.

Fink, M., and Kessler, J. (1963). *Z. Physik 174*, 197.

Glaser, W. (1952). "Grundlagen der Elektronenoptik," pp. 147 and 221. Springer, Vienna.

Glaser, W. (1956). In "Handbuch der Physik" (S. Flügge, ed.), Vol. 33, pp. 188 and 254. Springer, Berlin.

Glaser, W., and Schiske, P. (1954). *Optik* **11**, 422.

Glaser, W., and Schiske, P. (1955). *Optik* **12**, 233.

Gobrecht, R. (1941). *Arch. Elektrotech.* **35**, 672.

Gölz, E. (1940). *Jahrb. AEG Forsch.* **7**, 57.

Gribi, M., Thürkauf, M., Villiger, W., and Wegmann, L. (1959). *Optik* **16**, 65.

Grivet, P. (1958). "Optique Electronique," Vol. II, p. 170ff. Bordas, Paris; (engl. Edition: Electron Optics, Pergamon, Oxford, 1965).

Hahn, E. (1954). *Jenaer Jahrb.* **1954**, part 1, 63.

Hahn, E. (1958). *Jenaer Jahrb.* **1958**, part 1, 184.

Hahn, E. (1959). *Exptl. Tech. Physik* **7**, 258.

Hahn, E. (1961). *Jenaer Jahrb.* **1961**, part 2, 325.

Hahn, E. (1964). *Jenaer Jahrb.* 1964, 217.

Hamisch, H., and Oldenburg, K. (1964). *Proc. 3rd Regional Conf. Electron Microscopy, Prague, 1964*. Vol. A, p. 41. Publishing House of Czech. Acad. Sci., Prague.

Hanszen, K.-J. (1958a). *Optik* **15**, 304.

Hanszen, K.-J. (1958b). *Z. Naturforsch.* **13a**, 409.

Hanszen, K.-J. (1962). *Proc. 5th Intern. Conf., Electron Microscopy, Philadelphia, 1962*. Vol. I, KK 11. Academic Press, New York.

Hanszen, K.-J. (1964a). *Z. Naturforsch.* **19a**, 896.

Hanszen, K.-J. (1964b). *Naturwissenschaften* **51**, 379.

Hanszen, K.-J. (1964c). *Proc. 3rd Regional Conf. Electron Microscopy, Prague 1964*. Vol. A, p. 47. Publishing House of Czech. Acad. Sci., Prague.

Hanszen, K.-J., and Lauer, R. (1965). *Optik* **20**, *23*, 478.

Hartl, W. A. M. (1966). *Z. Physik.* **191**, 487.

Heise, F. (1949). *Optik* **5**, 479.

Heise, F., and Rang O., (1949). *Optik* **5**, 201.

Hoeft, J. (1959). *Z. Angew. Phys.* **11**, 380.

Hottenroth, G. (1937). *Ann. Physik* [5] **30**, 689.

Illenberger, A. (1964). *Mikroskopie* **19**, 316.

Jacob, L., and Shah, J. R. (1953). *J. Appl. Phys.* **24**, 1261.

Kanaya, K., Kawakatsu, H., Yamazaki, H., and Sibata, S. (1966). *J. Sci. Instr.* **43**, 416.

Kessler, J., and Lindner, H. (1964). *Z. Angew. Phys.* **18**, 7.

Klemperer, O., and Wright, W. D. (1939). *Proc. Phys. Soc.* (*London*) **51**, 296.

Kofoid, M. J. (1960a). *Power App. Systems* No. 51, 991.

Kofoid, M. J. (1960b). *Power App. Systems* No. 51, 999.

Laplume, J. (1947). *Cahiers Phys.* [5] **29-30**, 55.

Lauer, R., and Hanszen, K.-J. (1966). *6th Intern. Congress for Electron Microscopy, Kyoto*, Vol. I, p. 129.

Lauer, R. (1967). *Z. Naturforsch.* **22a**, in print.

Liebmann, G. (1949). *Proc. Phys. Soc.* (*London*) **B62**, 213.

Lippert, W. (1955a). *Optik* **12**, 173.

Lippert, W. (1955b). *Optik* **12**, 467.

Lippert, W., and Pohlit, W. (1952). *Optik* **9**, 456.

Lippert, W., and Pohlit, W. (1953). *Optik* **10**, 447.

Lippert, W., and Pohlit, W. (1954). *Optik* **11**, 181.

MacNaughton, M. M. (1952). *Proc. Phys. Soc.* (*London*) **B65**, 590.

Mahl, H. (1940). *Jahrb. AEG Forsch.* **7**, 43.

Mahl, H., and Recknagel, A. (1944). *Z. Physik* **122**, 660.

Metherell, A. J. F., and Whelan, M. J. (1966). *J. Appl. Phys.* **37**, 1737.

Miller, H. C. (1966). *J. Appl. Phys.* **37**, 784.

Möllenstedt, G., and Dietrich, W. (1955). *Optik* **12**, 246.

Möllenstedt, G., and Rang, O. (1951). *Z. Angew. Phys.* **3**, 187.

Nicoll, F. H. (1938). *Proc. Phys. Soc.* (*London*) **50**, 888.

Rabinowitz, M. (1965). *Vacuum* **15**, 59.

Rang, O. (1949). *Optik* **5**, 518.

Recknagel, A. (1941). *Z. Physik* **117**, 689.

Recknagel, A. (1943). *Z. Physik* **120**, 331.

Regenstreif, E. (1951). *Ann. Radioelec. Compagn. Franc. Assoc. T.S.F.* **6**, 51, 114, 245, and 299.

Schumacher, B. W. (1966). *Rev. Sci. Instr.* **8**, 1092.

Seeliger, R. (1948). *Optik* **4**, 258.

Septier, A. (1954a). *Ann. Radioelec. Compagn. Franc. Assoc. T.S.F.* **9**, 374.

Septier, A. (1954b). *J. Phys. Radium* [8] **15**, 573.

Septier, A. and Ruytoor, M. (1959). *Compt. Rend.* **249**, 2175.

Septier, A. (1960). *CERN Rept.* **60-39**.

Shipley, D. W. (1952). *J. Appl. Phys.* **23**, 1310.

Simpson, J. A., and Marton L. (1961). *Rev. Sci. Instr.* **32**, 802.

Soa, E. A. (1959). *Jenaer Jahrb.* **1959**, part 1, 115.

Spangenberg, K. L., and Field, L. M. (1942). *Proc. IRE* **30**, 138.

Verster, J. L. (1963). *Philips. Res. Rept.* **18**, 465.

Vine, J. (1960). *Brit. J. Appl. Phys.* **11**, 408.

von Ardenne, M. (1956). "Tabellen der Elektronenphysik, Ionenphysik und Übermikroskopie," Vol. I, p. 118. VEB Deutscher Verlag der Wissenschaften, Berlin.

von Ardenne, M. (1964). "Tabellen zur angewandten Physik," Vol. II. VEB Deutscher Verlag der Wissenschaften, Berlin.

Wendt, G. (1940). *Z. Physik* **116**, 436.